JACS
JOURNAL OF THE AMERICAN CHEMICAL SOCIETY

Subscriber access provided by American Chemical Society

Article

Light-Driven Molecular Motors: Stepwise Thermal Helix Inversion during Unidirectional Rotation of Sterically Overcrowded Biphenanthrylidenes

Matthijs K. J. ter Wiel, Richard A. van Delden, Auke Meetsma, and Ben L. Feringa

J. Am. Chem. Soc., **2005**, 127 (41), 14208-14222• DOI: 10.1021/ja052201e • Publication Date (Web): 23 September 2005

Downloaded from http://pubs.acs.org on March 25, 2009

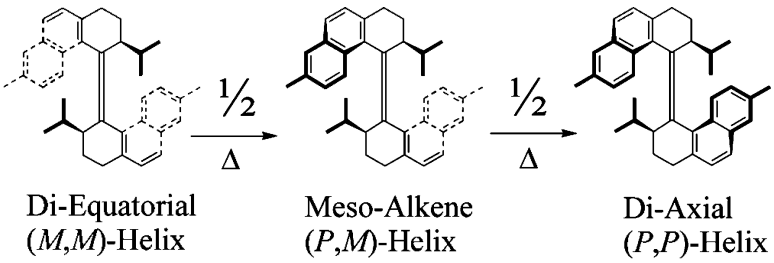

More About This Article

Additional resources and features associated with this article are available within the HTML version:

- Supporting Information
- Links to the 2 articles that cite this article, as of the time of this article download
- Access to high resolution figures
- Links to articles and content related to this article
- Copyright permission to reproduce figures and/or text from this article

View the Full Text HTML

ACS Publications
High quality. High impact.

Journal of the American Chemical Society is published by the American Chemical Society. 1155 Sixteenth Street N.W., Washington, DC 20036

J|A|C|S
ARTICLES
Published on Web 09/23/2005

Light-Driven Molecular Motors: Stepwise Thermal Helix Inversion during Unidirectional Rotation of Sterically Overcrowded Biphenanthrylidenes

Matthijs K. J. ter Wiel, Richard A. van Delden, Auke Meetsma, and Ben L. Feringa*

Contribution from the Department of Organic and Molecular Inorganic Chemistry, Stratingh Institute, University of Groningen, Nijenborgh 4, 9747 AG Groningen, The Netherlands

Received April 6, 2005; E-mail: b.l.feringa@rug.nl

Abstract: To investigate the unidirectional rotation of chiral overcrowded biphenanthrylidenes in more detail, the size of the substituent next to the double bond responsible for the unidirectionality of rotation was varied. The thermal and photochemical isomerization of three sterically overcrowded alkenes is described. The behavior of the biphenanthrylidenes with methyl and ethyl substituents is rather similar, and these compounds undergo a unidirectional 360° rotation around the central double bond in a four-step sequence involving two photochemical cis−trans isomerizations and two thermal helix inversions. The only difference between these two true molecular motors was a small entropic effect, which causes the ethyl substituted molecular motor to rotate slightly faster. The behavior of the *i*-propyl substituted compound differs significantly from that of the other two. Although not all different isomers of the *i*-propyl substituted molecular motor were detected spectroscopically, experimental data led to the conclusion that this compound can also be considered as a molecular motor and is capable of performing a 360° unidirectional rotation. ^{1}H NMR and X-ray analysis show a *meso*-like form as an intermediate in the unidirectional rotation, which proves that the thermal helix inversion is a stepwise process.

Introduction

The bottom-up construction of molecular motors,[1] in which controlled translational or rotational motion can be accomplished, offers a formidable contemporary challenge. Controlled motion is at the heart of the plethora of machinery our society depends on, and it is evident that there will be a key role for molecular motors in the development of nanotechnology ahead of us.[2] The fascinating molecular motors present in biological systems[3] such as the kinase linear motor[4] and the ATP-ase rotary motor[5] offer a great source of inspiration for the design of synthetic motors[6] in which a controllable motor function is present.

In synthetic approaches to construct molecular machinery[7] as part of the nanotechnology toolbox, systems have been devised in which an external chemical, electrochemical, or photochemical stimulus induces a switching process or movement within the molecules or triggers changes in shape or organization.[6−8] Among these systems are molecular propellers,[9] rotors,[10] brakes,[11] switches,[12] turnstiles,[13] ratchets,[14] shuttles,[15] elevators,[16] muscles,[17] scissors,[18] processive artificial enzymes,[19] and catalytic self-propelled micro- and nano-rods.[20]

To be able to construct a molecular rotary motor, we envision that three basic requirements need to be fulfilled: (i) repetitive 360° rotary motion; (ii) consumption of energy; and (iii) unidirectional rotation. In the first artificial molecular rotary motor systems,[21,22] a crucial factor is the control of the delicate

(1) Feynman, R. P. "There's plenty of room at the bottom − An invitation to enter a new field of physics." *Eng. Sci.* **1960**, February Issue.
(2) (a) *Encyclopedia of Nanoscience and Nanotechnology*; Singh, N. H., Ed.; American Scientific Publishers: Stevenson Ranch, CA, 2004. (b) *Nanotech, The Science of the Small Gets Down to Business*; *Scientific American*, Special Issue; September, 2004.
(3) *Molecular Motors*; Schliwa, M., Ed.; Wiley-VCH: Weinheim, 2003.
(4) Vale, R. D.; Milligan, R. A. *Science* **2000**, *88*, 88−94.
(5) (a) Boyer, P. D. *Angew. Chem., Int. Ed.* **1998**, *37*, 2296−2307. (b) Walker, J. E. *Angew. Chem., Int. Ed.* **1998**, *37*, 2308−2319.
(6) (a) *Molecular Catenanes, Rotaxanes, and Knots*; Sauvage, J.-P., Dietrich-Buchecker, C., Eds.; Wiley-VCH: Weinheim, 1999. (b) Balzani, V.; Gómez-López, M.; Stoddart, J. F. *Acc. Chem. Res.* **1998**, *31*, 405−414. (c) "Molecular Machines." Stoddart, J. F., Ed.; Special Issue. *Acc. Chem. Res.* **2000**, *100*, 409−522.
(7) (a) Venturi, M.; Credi, A.; Balzani, V. *Molecular Devices and Machines − A Journey into the Nanoworld*; Wiley-VCH: Weinheim, 2003. (b) Sauvage, J.-P. *Struct. Bond.* **2001**, *99*, 55−78.
(8) (a) Balzani, V.; Credi, A.; Raymo, F. M.; Stoddart, J. F. *Angew. Chem., Int. Ed.* **2000**, *39*, 3348−3391. (b) Feringa, B. L.; Koumura, N.; van Delden, R. A.; ter Wiel, M. K. J. *Appl. Phys. A* **2002**, *75*, 301−308.
(9) Iwamura, H.; Mislow, K. *Acc. Chem. Res.* **1988**, *21*, 175−182.
(10) (a) For a comprehensive review, see: Kottas, G. S.; Clarke, L. I.; Horinek, D.; Michl, J. *Chem. Rev.* **2005**, *105*, 1281−1376. (b) Schoevaars, A. M.; Kruizinga, W.; Zijlstra, R. W. J.; Veldman, N.; Spek, A. L.; Feringa, B. L. *J. Org. Chem.* **1997**, *62*, 4943−4948. (c) Dominguez, Z.; Dang, H.; Strouse, M. J.; Garcia-Garibay, M. A. *J. Am. Chem. Soc.* **2002**, *124*, 2398−2399. (d) Godlinez, C. E.; Zepada, G.; Garcia-Garibay, M. A. *J. Am. Chem.* Soc. **2002**, *124*, 4701−4707. (e) Dominguez, Z.; Dang, H.; Strouse, M. J.; Garcia-Garibay, M. A. *J. Am. Chem.* Soc. **2002**, *124*, 7719−7727. (f) Dominguez, Z.; Khuong, T.-A. V.; Dang, H.; Sanrame, C. N.; Nuñez, J. E.; Garcia-Garibay, M. A. *J. Am. Chem. Soc.* **2003**, *125*, 8827−8837. (g) Kuwatani, Y.; Yamamoto, G.; Iyoda, M. *Org. Lett.* **2003**, *5*, 3371−3374. (h) Carella, A.; Rapenne, G.; Launey, J.-P. *New J. Chem.* **2005**, *29*, 288−290. (i) Hawthorne, M. F.; Zink, J. I.; Skelton, J. M.; Bayer, M. J.; Liu, C.; Livshits, E.; Baer, R.; Neuhauser, D. *Science* **2004**, *303*, 1848−1851.
(11) Kelly, T. R.; Bowyer, M. C.; Bhaskar, K. V.; Bebbington, D.; Garcia, A.; Lang, F.; Kim, M. H.; Jette, M. P. *J. Am. Chem. Soc.* **1994**, *116*, 3657−3658.
(12) (a) *Molecular Switches*; Feringa, B. L., Ed.; Wiley-VCH: Weinheim, 2001. (b) "Photochromism: Memories and Switches." Irie, M., Ed.; Special Issue. *Chem. Rev.* **2000**, *100*, 1683−1890.
(13) Bedard, T. C.; Moore, J. S. *J. Am. Chem. Soc.* **1995**, *117*, 10662−10671.
(14) (a) Kelly, T. R.; Sestelo, J. P.; Tellitu, I. *J. Org. Chem.* **1998**, *63*, 3655−3665. (b) Harrington, L. E.; Cahill, L. S.; McGlinchey, M. J. *Organometallics* **2004**, *23*, 2884−2891.

10.1021/ja052201e CCC: $30.25 **© 2005 American Chemical Society**

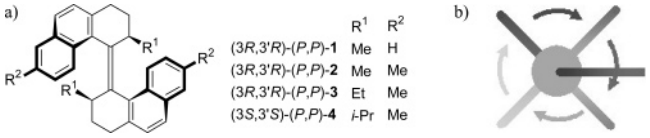

Figure 1. (a) Structures of the designed molecular motors. (b) Schematic representation of the 360° unidirectional rotation.

dynamic molecular chirality. This allowed repetitive unidirectional rotary motion (360°) powered by light as demonstrated in our laboratories[21] and chemical driven unidirectional rotation (120°) as shown by Kelly et al.[22] in a triptycene based motor. Leigh et al.[23] demonstrated unidirectional rotation in an ingenious mechanically interlocked molecular motor system, and they were able to demonstrate reversal of the rotary motion.[24] Other recent approaches include an electronically controllable, surface bound rotor[25] and a laser-induced aldehyde rotor.[26] It was also shown that the light-driven molecular motor was able to perform work[27] and that the rotary motion could be accelerated by structural modification.[28]

The first light-driven unidirectional rotary motor is based on chiral overcrowded alkene (3*R*,3′*R*)-(*P*,*P*)-*trans*-**1** (Figure 1a).[21] The design features two halves, one of which can be considered the stator part and the other the rotor part connected by a central olefinic moiety that functions as the axis of rotation. A full 360° rotation cycle of the rotor with respect to the stator part involves four distinct stages (Figure 1b). Examining the structure of **1**, it is evident that both a stereocenter, which has a fixed

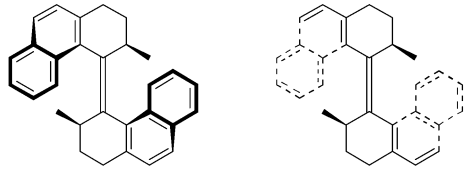

Figure 2. Relative stabilities of the stable and unstable *trans*-isomers of **1**.

stereochemistry, and a helical structure, the helicity of which can be changed by trans−cis photoisomerization, are present in the same molecule. An important feature is that the methyl substituents in **1** can adopt two distinct orientations, that is, (pseudo-)axial and (pseudo-)equatorial, which results in two distinct forms shown for *trans*-**1** in Figure 2. In the more stable (3*R*,3′*R*)-(*P*,*P*)-*trans*-**1**, the methyl substituents adopt (pseudo-)axial orientations, whereas in the less stable (3*R*,3′*R*)-(*M*,*M*)-*trans*-**1** the methyl substituents adopt (pseudo-)equatorial orientations. MOPAC93-AM1 calculations showed that the difference in stability of 35.9 kJ mol^{-1} is due to steric hindrance of the methyl groups in the unfavorable equatorial orientation. For the corresponding *cis*-isomers, a similar situation exists with a difference in stability of 46.0 kJ mol^{-1} for the stable and unstable forms.

The combination of two photochemical steps and two thermal isomerization steps completes the four-stage 360° rotary motion around the central double bond in **1**, whereas the difference in energy between the axial and equatorial orientations of the methyl substituents governs the unidirectionality. Because the photochemical steps are equilibria, the absolute stereochemistry of the motor molecules and the thermal processes fully account for the directionality of rotation around the central double bond. It should be noted that the thermal isomerization steps are also equilibria, but the equilibria are completely (>99%) on the side of the thermodynamically more stable isomers. The unstable forms of molecule **1**, generated photochemically, have their methyl substituents in the energetically unfavorable equatorial conformation. When these unstable molecules are heated, a thermal helix inversion occurs and simultaneously the methyl substituents adopt again their preferred, energetically more stable, axial orientation. This holds both for the *trans*- and for the *cis*-isomers. Although the presence of a substituent at the stereogenic center is not the only factor that contributes to the unidirectionality of the rotary movement, its preference for an axial conformation governs the direction of the two thermal steps in the rotation process and hence the direction of the rotary motion.

We report here a detailed study of the structural, stereochemical, and dynamic aspects associated with first generation rotary motors. It was decided to introduce substituents of different sizes at the stereogenic centers and study their effect on the delicate balance between conformational and steric effects with the intention to gain more insight into structural features that govern the photochemical and thermal isomerization processes. The behavior of the synthesized molecules might be rationalized beforehand in terms of steric hindrance during the thermal

(15) For examples of various molecular shuttles, see: (a) Steuermann, D. W.; Tseng, H.-R.; Peters, A. J.; Flood, A. H.; Jeppesen, J. O.; Nielsen, K. A.; Stoddart, J. F.; Heath, J. R. *Angew. Chem., Int. Ed.* **2004**, *43*, 6486−6491. (b) Tseng, H.-R.; Vignon, S. A.; Stoddart, J. F. *Angew. Chem., Int. Ed.* **2003**, *42*, 1491−1495. (c) Huang, T. J.; Tseng, H.-R.; Sha, L.; Lu, W.; Brough, B.; Flood, A. H.; Yu, B.-D.; Celestre, P. C.; Chang, J. P.; Stoddart, J. F.; Ho, C.-M. *Nano Lett.* **2004**, *4*, 2065−2071. (d) Ashton, P. R.; Baldoni, V.; Balzani, V.; Credi, A.; Hoffmann, H. D. A.; Martínez-Diaz, M.-V.; Raymo, F. M.; Stoddart, J. F.; Venturi, M. *Chem.-Eur. J.* **2001**, *7*, 3482−3493. (e) Bottari, G.; Leigh, D. A.; Pérez, E. M. *J. Am. Chem. Soc.* **2003**, *125*, 13360−13361. (f) Da Ros, T.; Guldi, D. M.; Farran Morales, A.; Leigh, D. A.; Prato, M.; Turco, R. *Org. Lett.* **2003**, *5*, 689−691. (g) Chang, S.-Y.; Jeong, K.-S. *J. Org. Chem.* **2003**, *68*, 4041−4049. (h) Altieri, A.; Gatti, F. G.; Kay, E. R.; Leigh, D. A.; Martel, D.; Paolucci, F.; Slawin, A. M. Z.; Wong, J. K. Y. *J. Am. Chem. Soc.* **2003**, *125*, 8644−8654. (i) Brouwer, A. M.; Frochot, C.; Gatti, F. G.; Leigh, D. A.; Mottier, L.; Paolucci, F.; Roffia, S.; Wurpel, G. W. H. *Science* **2001**, *291*, 2124−2128. (j) Jimenez-Molero, M. C.; Dietrich-Buchecker, C.; Sauvage, J.-P. *Chem.-Eur. J.* **2002**, *8*, 1456−1466.
(16) Badjić, J. D.; Balzani, V.; Credi, A.; Silvi, S.; Stoddart, J. F. *Science* **2004**, *303*, 1845−1849.
(17) Jiménez, M. C.; Dietrich-Buchecker, C.; Sauvage, J.-P. *Angew. Chem., Int. Ed.* **2000**, *39*, 3284−3287.
(18) Muraoka, T.; Kinbara, K.; Kobayashi, Y.; Aida, T. *J. Am. Chem. Soc.* **2003**, *125*, 5612−5613.
(19) Thordarson, P.; Bijsterveld, E. J. A.; Rowan, A. E.; Nolte, R. J. M. *Nature* **2003**, *424*, 915−918.
(20) (a) Ismagilov, R. F.; Schwartz, A.; Bowden, N.; Whitesides, G. M. *Angew. Chem., Int. Ed.* **2002**, *41*, 652−654. (b) Paxton, W. F.; Kistler, K. C.; Olmeda, C. C.; Sen, A.; St. Angelo, S. K.; Coa, Y.; Mallouk, T. E.; Lammert, P. E.; Crespi, V. H. *J. Am. Chem. Soc.* **2004**, *126*, 13424−13431. (c) Kline, T. R.; Paxton, W. F.; Mallouk, T. E.; Sen, A. *Angew. Chem., Int. Ed.* **2005**, *44*, 744−746. (d) Catchmark, J. M.; Subramanian, S.; Sen, A. *Small* **2005**, *1*, 202−206. (e) Fournier-Bidoz, S.; Arsenault, A. C.; Manners, I.; Ozin, G. A. *Chem. Commun.* **2005**, 441−443.
(21) Koumura, N.; Zijlstra, R. W. J.; van Delden, R. A.; Feringa, B. L. *Nature* **1999**, *401*, 152−155.
(22) Kelly, T. R.; De Silva, H.; Silva, R. A. *Nature* **1999**, *401*, 150−152.
(23) Leigh, D. A.; Wong, J. K. Y.; Dehez, F.; Zerbetto, F. *Nature* **2003**, *424*, 174−179.
(24) Hernández, J. V.; Kay, E. R.; Leigh, D. A. *Science* **2004**, *306*, 1532−1537.
(25) Zheng, X.; Mulcahy, M. E.; Horinek, D.; Galeotti, F.; Magnera, T. F.; Michl, J. *J. Am. Chem. Soc.* **2004**, *126*, 4540−4542.
(26) Hoki, K.; Yamaki, M.; Fujimura, Y. *Angew. Chem., Int. Ed.* **2003**, *43*, 2976−2978.
(27) van Delden, R. A.; Koumura, N.; Harada, N.; Feringa, B. L. *Proc. Natl. Acad. Sci. U.S.A.* **2002**, *99*, 4945−4949.
(28) ter Wiel, M. K. J.; van Delden, R. A.; Meetsma, A.; Feringa, B. L. *J. Am. Chem. Soc.* **2003**, *125*, 15076−10586.

Scheme 1. Synthesis of the Ketones **7**, **13**, and **14**

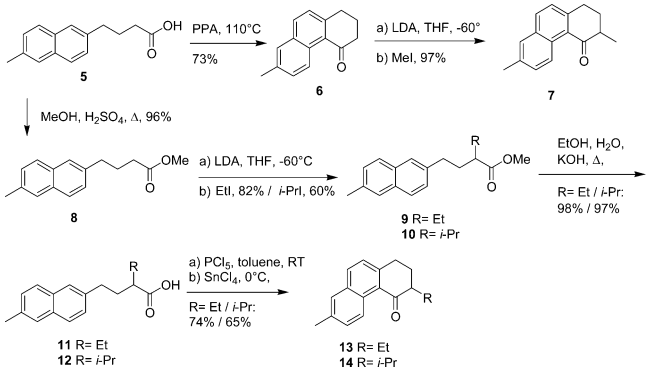

Scheme 2. Synthesis of the Molecular Motors **2**, **3**, and **4**

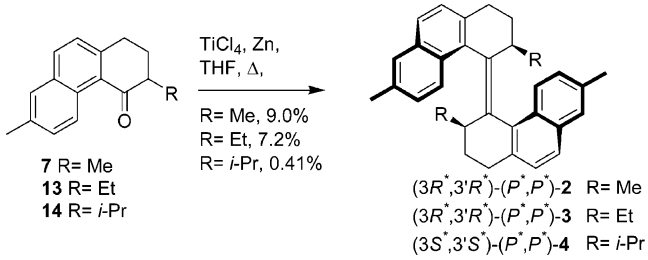

isomerization steps. It is expected that substituents R^1 of increasing size next to the central alkene moiety impose more steric hindrance onto the molecule in going from the methyl **2** to the ethyl **3** and the *i*-propyl **4** substituted compounds (Figure 1).[29] It must be noted, however, that it is our experience that it is difficult to predict what the effects of structural modifications will be on the ground states and on the excited states of the molecules.[30] A particular pertinent question is related to the mechanism of the rate-determining thermal helix inversion in these molecules, as this knowledge might also assist in the design of faster motors. If the molecular motors are to be used for further applications, they require additional functionalization, either at the naphthalene ring or at the aliphatic part of the molecule, without affecting the unidirectionality of rotation. The extra methyl substituent built into these molecules (R^2 = Me), at the 7-position of the naphthalene rings, is not only present for synthetic convenience, but also to examine whether these positions (providing the possibility to induce a large spatial change upon rotation) can be used to attach functionalities needed for future applications. Model studies indicate that a substituent in this position does not play a role in the rotary behavior, as it is remote from the "fjord-region" of the molecule.

Synthesis and Structural Analysis

The key step in the synthesis of chiral overcrowded biphenanthrylidenes **2**−**4** is the final step in the synthetic route in which two ketones are reductively coupled in a McMurry reaction (Scheme 1).[31] This reaction often results in low yields due to the severe steric hindrance that is introduced into the overcrowded product during the coupling.

The ketone precursors **7**, **13**, and **14**, however, can be readily obtained following straightforward methodology (Scheme 1). According to a protocol by Haworth et al.,[32] β-methylnaphthalene was converted in two steps to the carboxylic acid **5**. Subsequent cyclization using PPA gave ketone **6**, which then could be methylated in the β-position to provide **7** in good yield by deprotonation with LDA and subsequent reaction with methyl iodide at −60 °C in THF. Two ketones **7** were then coupled using a McMurry protocol in which a combination of $TiCl_4$ and Zn powder in THF was used to give the racemate of the desired motor molecule (3*R**,3′*R**)-(*P**,*P**)-**2**, albeit in low yield (Scheme 2).[33] Employing previously developed methodology involving an asymmetric methylation step,[34] enantiomerically pure (3*S*,3′*S*)−(*M*,*M*)-**2** was synthesized and used for the photochemical and thermal experiments which are described below.

For the synthesis of the ethyl **3** and *i*-propyl **4** substituted analogues, it may appear that direct alkylation of the enolate of **6** with ethyl iodide or *i*-propyl iodide would readily provide the desired substituted ketones. This strategy, however, proved to be less convenient due to dialkylation at the α-carbon. Therefore, a route was preferred in which the alkyl substituents were introduced in an earlier stage of the synthesis. The ester enolate of **8** was generated with LDA and quenched with the appropriate alkyl halide to provide the ethyl **9** and *i*-propyl **10** substituted esters in 82% and 60% yield, respectively. Hydrolysis of the esters **9** and **10** to the corresponding acids **11** and **12** was followed by reaction with PCl_5 to provide the acyl chlorides. These acyl chlorides were not isolated, but directly used in the following ring closure using $SnCl_4$, which gave phenanthrenones **13** and **14** in good yields (Scheme 1). With these ketones in hand, the stage was set for the most delicate reaction of the entire sequence: the coupling of two ketone moieties to form the overcrowded alkene in one step using the McMurry reaction. Although numerous sterically hindered alkenes have successfully been made using the McMurry reaction, the increased steric demand in the molecular motors **2**−**4** resulted in decreasing yield going from a methyl substituent to an *i*-propyl substituent. Various combinations of Zn and Ti reagents were employed in the reaction, but eventually the combination of $TiCl_4$ and Zn powder proved to be the most reliable and provided the *trans*-

(29) The overall conformation of the *i*-propyl substituted alkene **4** is identical to that of the methyl **2** and ethyl **3** substituted alkenes. However, due to an extra carbon present in the *i*-propyl substituent, the priority of the substituents attached to the stereogenic center alters. Therefore, the stable *trans*-isomer of **4** consists of the (3*S*,3′*S*)-(*P*,*P*)-*trans*-**4** and (3*R*,3′*R*)-(*M*,*M*)-*trans*-**4** enantiomers and not of the (3*S*,3′*S*)-(*M*,*M*)-*trans* and (3*R*,3′*R*)-(*P*,*P*)-*trans* enantiomers as is the case with stable *trans*-isomers of methyl **2** and ethyl **3** substituted alkenes.

(30) (a) van Delden, R. A.; ter Wiel, M. K. J.; de Jong, H.; Meetsma, A.; Feringa, B. L. *Org. Biomol. Chem.* **2004**, *2*, 1531−1541. (b) Geertsema, E. M.; Koumura, N.; ter Wiel, M. K. J.; Meetsma, A.; Feringa, B. L. *Chem. Commun.* **2002**, 2962−2963.

(31) (a) Fürstner, A.; Bogdanović, B. *Angew. Chem., Int Ed. Engl.* **1996**, *35*, 2442−2469. (b) Lectka, T. In *Active Metals; Chapter 3: The McMurry Reaction*; Fürstner, A., Ed.; VCH: Weinheim, 1996; pp 85−131. (c) McMurry, J. E. *Chem. Rev.* **1989**, *89*, 1513−1524. (d) McMurry, J. E. *Acc. Chem. Res.* **1983**, *16*, 405−411.

(32) Haworth, R. D.; Letsky, B. M.; Mavin, C. M. *J. Chem. Soc.* **1932**, 1784−1792.

(33) The use of an asterisk (*) throughout this paper denotes the use of racemic compounds and is used to clarify the relation between the helicity of the molecule and the absolute configuration of the carbon atom of the stereogenic center. For example, for an alkene with a methyl substituent, (3′*R**,3′*R**)-(*P**,*P**)-*trans* means that the alkene is a racemic mixture of two enantiomers, (3*R*,3′*R*)-(*P*,*P*)-*trans* and (3*S*,3′*S*)-(*M*,*M*)-*trans*, of a stable *trans*-isomer, whereas for the same alkene, (3*R**,3′*R**)-(*M**,*M**)-*trans* would indicate that the molecule is a racemic mixture of an unstable *trans*-isomer consisting of the (3*R*,3′*R*)-(*M*,*M*)-*trans* and (3*S*,3′*S*)-(*P*,*P*)-*trans* enantiomers. From this example, it is important to note that a combination of the absolute configuration at the stereogenic carbon atom (*R* or *S*) and the overall helicity of the molecule (*P* or *M*) is only valid for certain combinations, because different isomers, stable or unstable, can be meant.

(34) (a) ter Wiel, M. K. J.; Koumura, N.; van Delden, R. A.; Meetsma, A.; Harada, N.; Feringa, B. L. *Chirality* **2000**, *12*, 734−741. (b) ter Wiel, M. K. J.; Koumura, N.; van Delden, R. A.; Meetsma, A.; Harada, N.; Feringa, B. L. *Chirality* **2001**, *13*, 336.

Scheme 3. Photosynthesis of the *cis*-Isomers of **2** and **3**

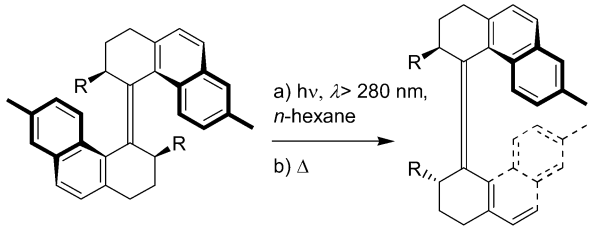

$(3R^*,3'R^*)$-(P^*,P^*)-**2** R= Me
$(3R^*,3'R^*)$-(P^*,P^*)-**3** R= Et

$(3R^*,3'R^*)$-(P^*,P^*)-**2** R= Me
$(3R^*,3'R^*)$-(P^*,P^*)-**3** R= Et

alkenes-**2**, -**3**, and -**4** in 9.0%, 7.0%, and 0.41% yield, respectively (Scheme 2).[33] Especially in case of olefin **4**, purification was severely complicated by the formation of apolar side-products.[35] It is difficult to account for the sole formation of *trans*-isomers in all three cases, as the mechanistic picture for the McMurry reaction is quite complicated. Besides the generally accepted mechanism, coupling of two ketyl radicals followed by elimination of the titanium oxo-species, recent experiments suggest that titanium alkylidene species might be involved in the reaction.[36]

Another remarkable feature is that, during the reaction, a diastereomerically pure mixture of (*R*,*R*)- and (*S*,*S*)-olefins is formed. Because racemic ketones are used, the resultant olefin would be expected to be a statistical mixture of (*R*,*R*), (*S*,*S*), (*S*,*R*), and (*R*,*S*) coupled products, but the (*R*,*S*)- and (*S*,*R*)-isomers are not formed. Previous observations showed that racemization does not occur during the McMurry reaction of six-membered cyclic ketones.[34] However, it remains to be established which mechanism accounts for the observed selectivity in the formation of the alkenes.

To obtain the stable *cis*-isomers of the compounds studied, *n*-hexane solutions of the corresponding pure *trans*-isomers were irradiated ($\lambda \geq 280$ nm, at low temperature, $T = -40$ °C; for more details on photochemistry, see below). After irradiation of the sample and heating at 60 °C for 2 h with exclusion of light, ^{1}H NMR analysis revealed the formation of new isomeric products that were separated by preparative HPLC (silica, heptane) and proved to be the stable *cis*-isomers of **2** and **3** (Scheme 3). No *cis*-isomer of **4** was isolated due to reasons that will be explained later.

From the ^{1}H and ^{13}C NMR spectra, the C_2-symmetric nature in solution is evident for all three new motors, *trans*-**2**, -**3**, and -**4**. The *trans*-geometry of the molecule was assigned by comparison of the ^{1}H NMR with the original motor molecule **1** and was thoroughly established by ^{1}H NMR, COSY, and NOESY spectra (cf., Figure 4). Indicative for the *trans*-geometry of the molecules are the NOE interactions observed between H_5 and $H_{5'}$ in the aromatic region at δ 8.3 ppm, on one hand, and the protons at the stereogenic carbon atoms $C_{3'}$ and C_3 and present in the methyl substituents ($C_{3'ax}$ and C_{3ax}) attached to the stereogenic centers, on the other hand, for all three trans molecular motors **2**, **3**, and **4** (Figure 3).

Because of the complicated ^{1}H NMR spectra of the molecular motors, X-ray analyses were performed on single crystals of (3*S*,3′*S*)-(*M*,*M*)-*trans*-**2**, (3*R**,3′*R**)-(*P**,*P**)-*trans*-**3**, and

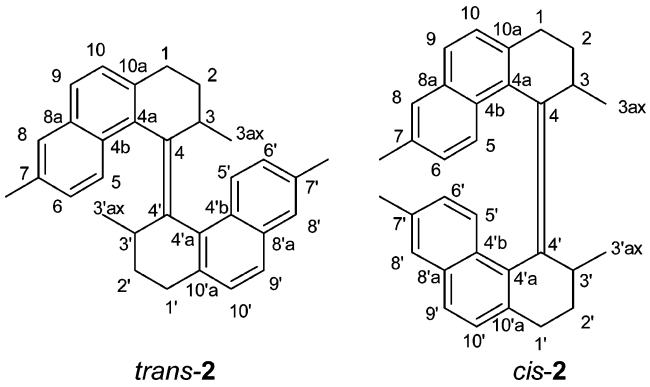

Figure 3. Numbering scheme adopted for the *trans*- (left) and *cis*-isomers (right) of the molecular motors described in this paper; here, methyl substituted **2** is depicted.

(3*S**,3′*S**)-(*P**,*P**)-*trans*-**4** to obtain definitive information about the geometry of the molecules, but most important to elucidate the crucial conformation of the substituents at the stereogenic centers C_3 and $C_{3'}$ in **2**−**4**.[35,37] Although the investigated crystal of (3*S**,3′*S**)-(*P**,*P**)-*trans*-**4** contained two residues with a slightly different conformation and opposite absolute configuration, all three structures were C_2-symmetric in the solid state like the structures observed in solution. As is exemplified with the Pluto structures of (3*S*,3′*S*)-(*M*,*M*)-*trans*-**2**, (3*R**,3′*R**)-(*P**,*P**)-*trans*-**3**, and (3*S**,3′*S**)-(*P**,*P**)-*trans*-**4** depicted in Figures 5−7, common features of these alkenes are their helical shape due to the steric crowding around the central double bond and the axial orientation of the methyl, ethyl, and *i*-propyl substituents. In all three structures, the naphthalene moiety and the alkyl substituent point in the same direction with respect to the central double bond. The conformation of the cyclohexene ring is, as predicted, severely twisted. For all compounds, this cyclohexene ring adopts a semi boatlike conformation. At this point, it should be emphasized that the structure of the molecule in the solid state does not necessarily give the correct structure of the motor molecules in solution, as small deviations can be expected with respect to the orientation around the double bond and the angle between the two naphthalene moieties.

The length of the central olefinic bond ranging from 1.341 to 1.355 Å in *trans*-**2**, -**3**, and -**4** deviates only slightly from the length of a normal olefinic bond of 1.33 Å.[38] Not surprisingly, the length of the central double bond in the most sterically hindered olefin, the *i*-propyl substituted compound **4**, is found to have the largest value (1.355 Å) of the three olefins. Nevertheless, the central olefinic bond is not severely twisted as can be seen from the angles around C_4: $C_3-C_4-C_{4a}$ (111.22°), $C_3-C_4-C_{4'}$ (122.76°), and $C_{4a}-C_4-C_{4'}$ (123.18°); and the torsion angles around the central double bond, $C_3-C_4-C_{4'}-C_{3'}$ (−146.48°), $C_3-C_4-C_{4'}-C_{4'a}$ (12.8°), and $C_{4a}-C_4-C_{4'}-C_{4'a}$ (172.01°). It is difficult to deduce directly the twist of the central olefinic bond from the torsion angles, but the Newman projections depicted in Figure 8 are particularly illustrative.

Like the *trans*-isomers of the molecules, the preferred C_2-symmetry of *cis*-**2** and *cis*-**3** in solution is immediately apparent from the ^{1}H NMR spectra of the molecules. The ^{1}H NMR

(35) See the Supporting Information for more detailed information.
(36) (a) Villiers, C.; Vandais, A.; Ephritikhine, M. *J. Organomet. Chem*. **2001**, *617*−*618*, 744−747. (b) Villiers, C.; Ephritikhine, M. *Chem.-Eur. J*. **2001**, *7*, 3043−3051. (c) Villiers, C.; Ephritikhine, M. *Angew. Chem., Int. Ed. Engl*. **1997**, *36*, 2380−2382.
(37) See ref 34; the crystal structure of (3*S*,3′*S*)-(*M*,*M*)-*trans*-**2** has been published previously and is included here for comparison.
(38) *CRC Handbook of Chemistry and Physics*; Lide, D. R., Ed.; CRC Press: Boca Raton, FL, 1993; Vol. 74, p 9-4.

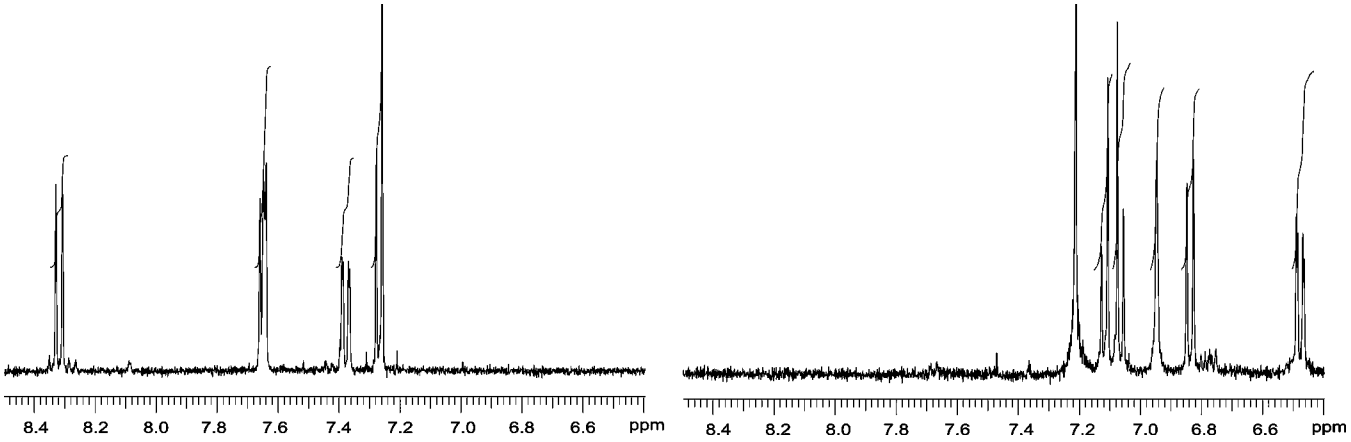

Figure 4. The aromatic region of the ^{1}H NMR spectra of *trans*-**2** (left) and *cis*-**2** (right).

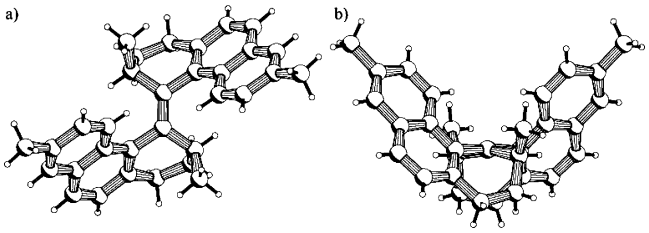

Figure 5. Pluto drawings of (3*S*,3′*S*)-(*M*,*M*)-*trans*-**2** seen perpendicular to the central double bond (a) and along the central double bond (b).

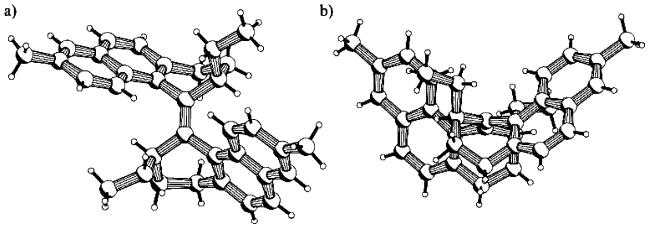

Figure 6. Pluto drawings of (3*R**,3′*R**)-(*P**,*P**)-*trans*-**3** seen perpendicular to the central double bond (a) and along the central double bond (b). The structures do not express the absolute stereochemistry of the molecule.

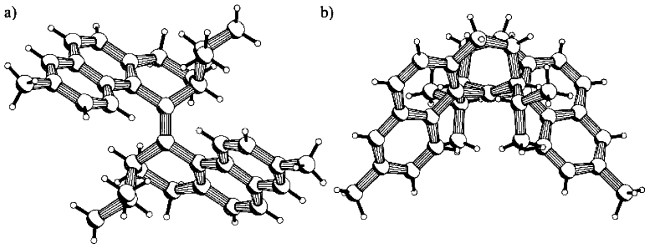

Figure 7. Pluto drawings of (3*S**,3′*S**)-(*P**,*P**)-*trans*-**4** seen perpendicular to the central double bond (a) and along the central double bond (b). The structures do not express the absolute stereochemistry of the molecule.

spectrum of *cis*-**2** is depicted in Figure 4. Absorptions of the aromatic protons are observed at relatively high field, at approximately δ 6.5 ppm for both *cis*-**2** and *cis*-**3**, which is the result of the ring current anisotropy experienced by these protons due to the close proximity of the naphthalene moiety in the other half of the molecule. A similar trend in the chemical shift of the aromatic protons was found for **1**.[39] Furthermore, NOE interactions were no longer observed between the protons of the substituent at the α-position (C_{3ax} and $C_{3'ax}$) and the proton in the equatorial position of the stereogenic carbon atom (H_{3eq} and $H_{3'eq}$) on one side and a proton in the naphthalene moiety of the molecule (H_5 and $H_{5'}$) on the other side (Figure 3). Unfortunately, NMR experiments did not give conclusive information about the geometry of the molecule. This is due to the highly complex splitting pattern in the aliphatic part of the molecule as well as the unusual conformation of the cyclohexene ring, for which the Karplus equation is of limited use.[40] Therefore, X-ray analyses of methyl substituted stable *cis*-**2** and ethyl substituted stable *cis*-**3** were performed.[35]

(39) Harada, N.; Koumura, N.; Feringa, B. L. *J. Am. Chem. Soc.* **1997**, *119*, 7256−7264.

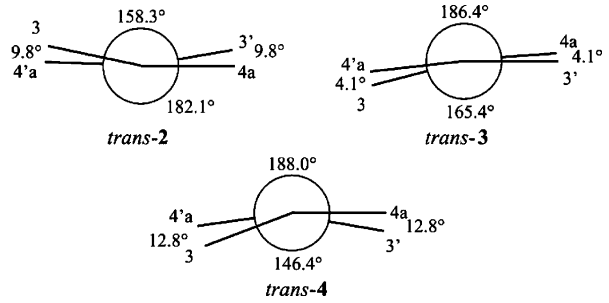

Figure 8. Newman projections of the central double bond of *trans*-**2**, -**3**, and -**4**.

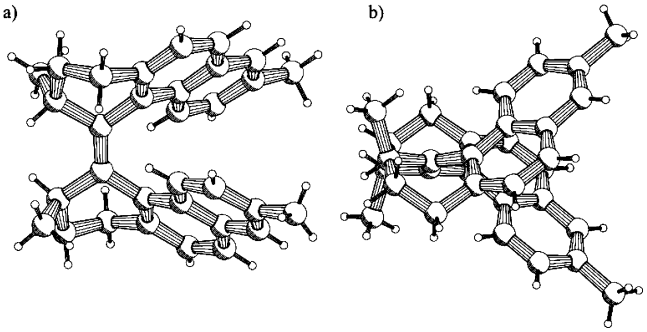

Figure 9. Pluto drawings of (3*R**,3′*R**)-(*P**,*P**)-*cis*-**2** seen perpendicular to the central double bond (a) and along the central double bond (b). The structures do not express the absolute stereochemistry of the molecule.

The first impression from the X-ray structure of (3*R**,3′*R**)-(*P**,*P**)-*cis*-**2** and (3*R**,3′*R**)-(*P**,*P**)-*cis*-**3** (Figures 9 and 10) is that both compounds are C_2-symmetric in the solid state, as was shown in solution by NMR. However, detailed analysis of the X-ray data of both *cis*-**2** and *cis*-**3** revealed in the solid state small distortions from the preferred C_2-symmetry (attributed to crystal packing effects). Common features of the two structures

(40) Karplus, M. *J. Am. Chem. Soc.* **1963**, *85*, 2870−2871.

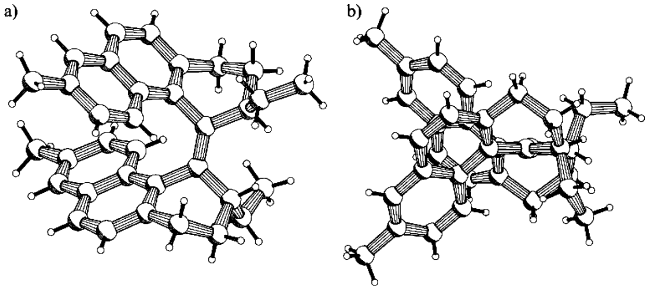

Figure 10. Pluto drawings of (3*R**,3′*R**)-(*P**,*P**)-*cis*-**3** seen perpendicular to the central double bond (a) and along the central double bond (b). The structures depicted do not express the absolute stereochemistry of the molecule.

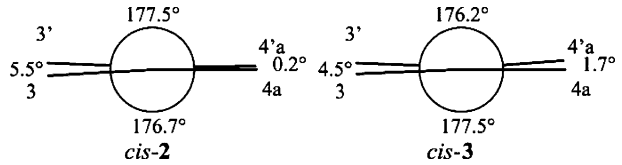

Figure 11. Newman projections of the central double bond of *cis*-**2** and -**3**.

are the helical shape of the molecule due to the steric hindrance, the axial orientation of the alkyl substituents at the stereogenic carbon center, as well as that these substituents and the naphthalene moieties point in the same direction with respect to the central double bond. Also, the cyclohexene ring in both structures adopts a semi boatlike conformation. Like in the *trans*-isomers, the central double bond in both the *cis*-methyl **2** (1.347 Å) and the *cis*-ethyl substituted olefin **3** (1.352 Å) was found to be slightly elongated as compared to the average value of 1.33 Å.[38] Most remarkable is that unlike all three stable trans forms of **2**, **3**, and **4**, the central double bond is hardly twisted, as is apparent from the torsion angles in *cis*-**2**: $C_3-C_4-C_{4'}-C_{3'}$ (5.5°), $C_3-C_4-C_{4'}-C_{4'a}$ (−176.9°), $C_{3'}-C_{4'}-C_4-C_{4a}$ (−177.8°), and $C_{4a}-C_4-C_{4'}-C_{4'a}$ (−0.2°). Only small deviations from planarity were found for the stable *cis*-isomers of **2** and **3**, as can be seen more clearly from the Newman projections in Figure 11.

Rotation Experiments

Based on our experience with the prototype molecular motor **1**, the anticipated 360° rotation around the central double bond of the new motor molecules takes place in four steps, as is depicted in Scheme 4.

In the first step of the 360° unidirectional rotation, the stable *trans*-isomer of the molecular motors, with both substituents in a (pseudo-)axial orientation, is irradiated at low temperature. During this energetically uphill process, a trans−cis photoisomerization of the alkene takes place to yield an isomer with a *cis*-geometry. The photochemical isomerization is reversible, and the composition of the photostationary states (ratio of stable and unstable isomers), which depends on the structures of the motors, is discussed for each motor further on. A consequence of the photoisomerization is that the orientation of the methyl substituents changes from a (pseudo-)axial orientation in the stable *trans*-isomer to a (pseudo-)equatorial orientation in the newly formed *cis*-isomer. Due to the enhanced steric constraints, the (pseudo-)equatorial orientation of the substituent is energetically unfavorable and these *cis*-isomers are kinetically labile. In the second step, a thermally induced helix inversion of the

Scheme 4. Photochemical and Thermal Isomerization Processes during the 360° Unidirectional Rotary Cycle for the Molecular Motors **2**, **3**, and **4**

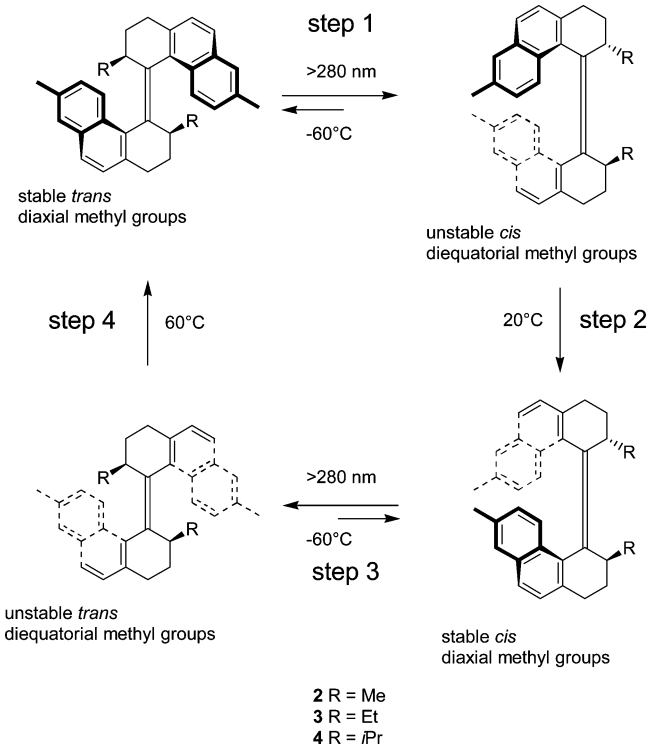

molecule takes place, which converts the unstable *cis*-isomer with its (pseudo-)equatorial substituents to a stable *cis*-isomer with the substituents in a (pseudo-)axial orientation. In the third step of the rotary process, a second energetically uphill cis−trans photoisomerization takes place. During the photoisomerization, the stable *cis*-isomer, with the substituents in a (pseudo-)axial position, undergoes a helix inversion and is converted to the unstable *trans*-isomer with its substituents in a (pseudo-)equatorial orientation. This isomer is again less stable due to the (pseudo-)equatorial orientation of the substituents. The unstable *trans*-isomer is converted upon heating to the stable *trans*-isomer, which has the substituents in the energetically favored (pseudo-)axial orientation. After the second thermal step, which is the fourth step in the entire rotary scheme, the stable *trans*-isomer is obtained again. In a four-step process, with light as the source of energy and by control of directionality via the changes in the orientation of the substituents, a unidirectional rotation around the central double bond has been accomplished.

Rotation Cycle for the Methyl Substituted Molecular Motor. To establish whether **2**, **3**, and **4** are indeed able to perform a unidirectional rotation around their central double bond, photochemical studies, similar to those of the original motor molecule **1**,[21] were performed. The UV−vis and CD spectra of enantiomerically pure (3*S*,3′*S*)-(*M*,*M*)-*trans*-**2**, prepared as described,[34] are depicted in Figures 12 and 13, respectively.[41] The UV−vis and CD characteristics of (3*S*,3′*S*)-(*M*,*M*)-*trans*-**2** are very similar to those of the original motor (3*R*,3′*R*)-(*P*,*P*)-*trans*-**1**. The most important features in the CD

(41) The absolute configuration of the enantiomerically pure alkene (3*S*,3′*S*)-(*M*,*M*)-*trans*-**2** was assigned on the basis of the stereochemical control excerted by the Evans' auxiliary. The assigned configuration was confirmed by comparison of the CD spectra of (3*S*,3′*S*)-(*M*,*M*)-*trans*-**2** and (3*R*,3′*R*)-(*P*,*P*)-*trans*-**1** and the CD spectra of the parent ketones.

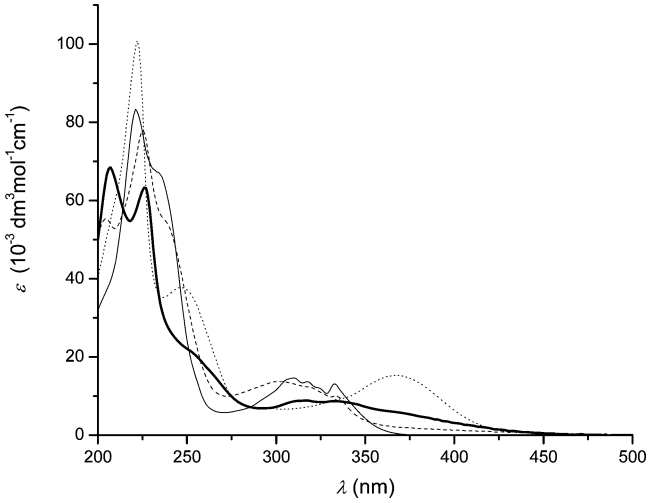

Figure 12. UV−vis spectra (*n*-hexane) observed during the rotary cycle **2**: (3*S*,3′*S*)-(*M*,*M*)-*trans*-**2** (thin solid); (3*S*,3′*S*)-(*P*,*P*)-*cis*-**2** (thick solid); (3*S*,3′*S*)-(*M*,*M*)-*cis*-**2** (dashed); (3*S*,3′*S*)-(*P*,*P*)-*trans*-**2** (dotted).

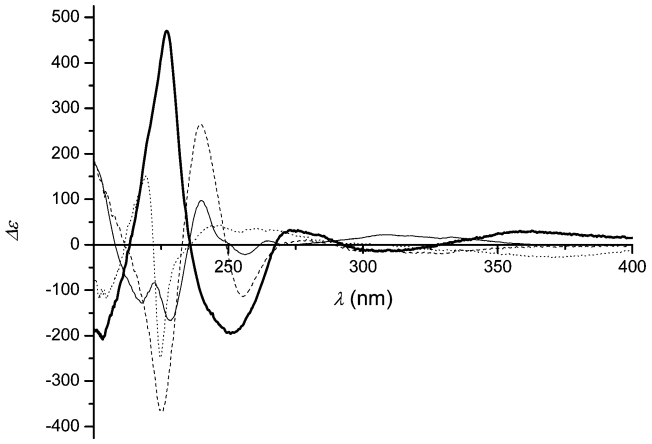

Figure 13. CD spectra (*n*-hexane) observed during the rotary cycle of **2**: (3*S*,3′*S*)-(*M*,*M*)-*trans*-**2** (thin solid); (3*S*,3′*S*)-(*P*,*P*)-*cis*-**2** (thick solid); (3*S*,3′*S*)-(*M*,*M*)-*cis*-**2** (dashed); (3*S*,3′*S*)-(*P*,*P*)-*trans*-**2** (dotted).

spectrum of (3*S*,3′*S*)-(*M*,*M*)-*trans*-**2** are the intense Cotton effects at 218, 229, and 240 nm. Photoisomerization of a solution in *n*-hexane of the stable (3*S*,3′*S*)-(*M*,*M*)-*trans*-**2** ($\lambda \geq 280$ nm, $T = -60$ °C) was monitored by UV−vis (Figure 12) and CD spectroscopy (Figure 13). The irradiation of the sample was continued until the photostationary state (PSS) had been reached.[42] In the UV−vis spectrum for the major absorptions at 221 and 233 nm, a small hypsochromic shift was observed and the two major absorption bands were found at 207 and 226 nm. The lowest energy absorption band showed a bathochromic shift as far as 420 nm. The photoisomerization could easily be followed, because the sample developed a yellow color during the irradiation. In the CD spectrum, an inversion in sign of most absorptions was observed, as well as a drastic increase in the value of the $\Delta\epsilon$. The values for $\Delta\epsilon$ were as high as +470.5 at 227.2 nm and −195.5 at 251.0 nm. The overall inversion in sign of the CD spectrum is indicative for the helix inversion of the molecule going from an overall (*M*)-helix in (3*S*,3′*S*)-(*M*,*M*)-*trans*-**2** to an overall (*P*)-helix in the new isomer formed upon irradiation. From the UV−vis and CD data, it was concluded that this new isomer is the anticipated unstable (3*S*,3′*S*)-(*P*,*P*)-*cis*-**2**, which has both methyl substituents in a (pseudo-)equatorial orientation and has an opposite helicity as compared to (3*S*,3′*S*)-(*M*,*M*)-*trans*-**2** (Scheme 4). Due to the thermal instability of (3*S*,3′*S*)-(*P*,*P*)-*cis*-**2**, the ratio between (3*S*,3′*S*)-(*M*,*M*)-*trans*-**2** and (3*S*,3′*S*)-(*P*,*P*)-*cis*-**2** at the PSS could not be determined directly (vide infra). The sample was therefore heated in the dark at 20 °C while the change of the CD absorption at 218 nm was monitored in time. When no further changes were observed, UV−vis and CD spectra were recorded. In the UV−vis spectrum, relatively small differences were seen, but the overall shape of the CD spectum was largely inverted and showed intense Cotton effects at 225.4 nm ($\Delta\epsilon = -367.5$) and 240.2 nm ($\Delta\epsilon = +264.3$). The overall change in sign of the CD spectrum is indicative for the helix inversion taking place upon heating. It was concluded that the unstable (3*S*,3′*S*)-(*P*,*P*)-*cis*-**2** had been converted to the stable (3*S*,3′*S*)-(*M*,*M*)-*cis*-**2**, in which the substituents have regained their energetically favorable (pseudo-)axial orientation. The conclusion that stable (3*S*,3′*S*)-(*M*,*M*)-*cis*-**2** has been formed was confirmed by HPLC and ^{1}H NMR analysis by comparison with material obtained from the synthesis described above. As already indicated, the composition of the mixture consisting of (3*S*,3′*S*)-(*P*,*P*)-*cis*-**2** and (3*S*,3′*S*)-(*M*,*M*)-*trans*-**2** at the first PSS could not be determined directly. After heating, however, the thermally stable (3*S*,3′*S*)-(*M*,*M*)-*trans*-**2** has been unaffected, while the unstable (3*S*,3′*S*)-(*P*,*P*)-*cis*-**2** is completely converted to the stable (3*S*,3′*S*)-(*M*,*M*)-*cis*-**2**. The ratio of isomers was determined by HPLC to be 85:15 and directly reflects the composition of the mixture of (3*S*,3′*S*)-(*P*,*P*)-*cis*-**2** and (3*S*,3′*S*)-(*M*,*M*)-*trans*-**2** at the PSS. The conversion of unstable (3*S*,3′*S*)-(*P*,*P*)-*cis*-**2** to stable (3*S*,3′*S*)-(*M*,*M*)-*cis*-**2** was monitored by CD spectroscopy in time at various temperatures. The Eyring equation, a plot of $\ln(k \cdot h)/(k_B \cdot T)$ versus $(1/T)$, allows the determination of various parameters for the activation barrier of the thermal helix inversion.[35] For the conversion of unstable (3*S*,3′*S*)-(*P*,*P*)-*cis*-**2** to stable (3*S*,3′*S*)-(*M*,*M*)-*cis*-**2**, the Gibbs energy of activation ($\Delta^{\ddagger}G^{\theta} = 91 \pm 3$ kJ mol^{-1}), the enthalpy of activation ($\Delta^{\ddagger}H^{\theta} = 69 \pm 3$ kJ mol^{-1}), and the entropy of activation ($\Delta^{\ddagger}S^{\theta} = -74 \pm 11$ J K^{-1} mol^{-1}) could be determined. The half-life of the process was calculated from the Gibbs energy of activation and was determined to be 32 min at room temperature (293.15 K).

The solution obtained after the first photoisomerization and the subsequent thermal helix inversion, containing a mixture of stable (3*S*,3′*S*)-(*M*,*M*)-*cis*-**2** and a small amount of stable (3*S*,3′*S*)-(*M*,*M*)-*trans*-**2**, was subjected to a second photochemical isomerization. The sample was therefore irradiated at low temperature ($\lambda \geq 280$ nm, $T = -60$ °C), and the conversion was followed by UV−vis. When the PSS was reached, UV−vis and CD spectra were recorded. In the UV−vis spectrum, a large increase in intensity was observed for the absorption band at 367 nm ($\lambda = 15\,300$). In the CD spectrum, the absorption of stable (3*S*,3′*S*)-(*M*,*M*)-*cis*-**2** at 225.4 nm ($\Delta\epsilon = -367.5$) was inverted to give a positive Cotton effect at 219.4 nm ($\Delta\epsilon = +151.0$). The inversion of the CD spectrum is again indicative for the change in helicity of the molecule going from an overall

(42) A chemoselective photoisomerization takes place as is evident from NMR analysis and the observation of clear isosbestic points in UV−vis and CD measurements during the photochemical steps. The quantum yields for the photochemical steps of motors **2**−**4** have not been determined yet. For molecular switches based on structurally related sterically overcrowded alkenes, quantum yields for photoisomerization in the range of 0.07−0.55, depending on the structure and solvent used, were found (Jager, W. F. Ph.D. Thesis, University of Groningen, 1994).

(*M*)-helicity in the stable (3*S*,3′*S*)-(*M*,*M*)-*cis*-**2** to an overall (*P*)-helicity in the newly formed isomer. From the UV−vis and CD data and by comparison with HPLC and ^{1}H NMR data, it was concluded that this newly formed isomer was the anticipated unstable (3*S*,3*S*′)-(*P*,*P*)-*trans*-**2**. The (3*S*,3*S*′)-(*P*,*P*)-*trans*-**2** isomer appeared to be relatively stable at room temperature, because no change in the CD signal at 20 °C was observed after several hours. The ratio between unstable (3*S*,3′*S*)-(*P*,*P*)-*trans*-**2** and stable (3*S*,3′*S*)-(*M*,*M*)-*cis*-**2** of 92:8 was directly determined independently by HPLC by irradiation of a sample of pure (3*S*,3′*S*)-(*M*,*M*)-*cis*-**2** in *n*-hexane ($\lambda \geq 280$ nm, $T = -60$ °C). Finally, the solution was heated in the dark at 60 °C, and the change in CD absorption was monitored at 218 nm. When no further changes were observed, UV−vis and CD spectra were recorded. These spectra indicated that a thermal helix inversion has taken place and that the molecule was converted into the original (3*S*,3′*S*)-(*M*,*M*)-*trans*-**2** isomer, demonstrating the unidirectional rotation around the central double bond in four consecutive steps.

During the second thermal helix conversion, going from unstable (3*S*,3*S*′)-(*P*,*P*)-*trans*-**2** to stable (3*S*,3*S*′)-(*M*,*M*)-*trans*-**2**, no thermodynamic data were acquired in *n*-hexane due to the relatively low rate of the process at 60 °C and the volatility of *n*-hexane.[43] The thermodynamic parameters were therefore obtained by using a solution of pure (3*S*,3′*S*′)-(*M*,*M*)-*cis*-**2** in dodecane. A solution of (3*S*,3′*S*)-(*M*,*M*)-*cis*-**2** was irradiated to form (3*S*,3′*S*′)-(*P*,*P*)-*trans*-**2** until no more change in the UV−vis spectrum could be observed ($\lambda \geq 280$ nm, $T = -20$ °C). By monitoring the change of the CD signal at 256 nm in time at various temperatures, the Gibbs energy ($\Delta^{\ddagger}G^{\theta} = 107 \pm 4$ kJ mol^{-1}), the enthalpy ($\Delta^{\ddagger}H^{\theta} = 86 \pm 4$ kJ mol^{-1}), and the entropy ($\Delta^{\ddagger}S^{\theta} = -73 \pm 16$ J K^{-1} mol^{-1}) of activation could be determined by making use of the Eyring equation.[35] The half-life of the unstable (3*S*,3′*S*)-(*P*,*P*)-*trans*-**2** was calculated to be 439 h at room temperature (293.15 K).

Rotation Cycle for the Ethyl Substituted Molecular Motor. The racemate of the ethyl substituted molecular motor (3*R**,3′*R**)-(*P**,*P**)-*trans*-**3** was resolved into its enantiomers by preparative HPLC (Chiralpack OD, *n*-hexane:*i*-propanol = 99.9:0.1). The absolute configuration of the isomer in the first eluted fraction was assigned to be (3*R*,3′*R*)-(*P*,*P*)-*trans*-**3** by comparison of the CD spectrum with those of the methyl substituted molecular motors (3*R*,3′*R*)-(*P*,*P*)-*trans*-**1** and (3*S*,3′*S*)-(*M*,*M*)-*trans*-**2**. The pseudo-enantiomeric relation between (3*R*,3′*R*)-(*P*,*P*)-*trans*-**3** and (3*S*,3′*S*)-(*M*,*M*)-*trans*-**2** can be seen clearly by comparison of the CD spectra of the molecules (Figures 13 and 15), which are nearly mirror images.

Although the barriers for the two thermal helix inversion steps are somewhat different for motor **3** than for motor **2**, the unidirectional 360° rotary processes are identical. The UV−vis and CD spectra of the four isomers are depicted in Figures 14 and 15. The rotary cycle starts with irradiation of (3*R*,3′*R*)-(*P*,*P*)-*trans*-**3** at low temperature ($\lambda \geq 280$ nm, $T = -60$ °C) to form the unstable (3*R*,3′*R*)-(*M*,*M*)-*cis*-**3**. Heating of this unstable isomer resulted in complete conversion to the stable (3*R*,3′*R*)-(*P*,*P*)-*cis*-**3**, as was apparent from ^{1}H NMR, UV−vis, CD, and HPLC data. After the sample was warmed to ensure complete conversion of the unstable *cis*-**3**, the ratio between the stable *trans*-**3** and stable *cis*-**3**, reflecting the composition at the PSS, was determined by HPLC and proved to be 3:97. By monitoring the thermal helix inversion at various temperatures, the activation parameters of the process could be determined ($\Delta^{\ddagger}G^{\theta} = 91 \pm 2$ kJ mol^{-1}, $\Delta^{\ddagger}H^{\theta} = 79 \pm 1$ kJ mol^{-1}, and $\Delta^{\ddagger}S^{\theta} = -35 \pm 2$ J K^{-1} mol^{-1}).[35] The half-life of the conversion of (3*R*,3′*R*)-(*M*,*M*)-*cis*-**3** to (3*R*,3′*R*)-(*P*,*P*)-*cis*-**3** was then calculated from the Gibbs energy of activation and proved to be 18 min at room temperature (293.15 K). A second irradiation resulted in the formation of the unstable (3*R*,3′*R*)-(*M*,*M*)-*trans*-**3**. The ratio at the PSS of (3*R*,3′*R*)-(*P*,*P*)-*cis*-**3** and (3*R*,3′*R*)-(*M*,*M*)-*trans*-**3** (stable *cis*-**3**:unstable *trans*-**3** = 5:95) was determined independently by irradiation of a sample of pure (3*R*,3′*R*)-(*P*,*P*)-*cis*-**3** ($\lambda \geq 280$ nm, $T = -60$ °C). Because unstable *trans*-**3** is relatively stable as compared to unstable *cis*-**3**, the ratio could be determined directly by HPLC analysis. Experiments performed in dodecane allowed the determination of the thermodynamic parameters ($\Delta^{\ddagger}G^{\theta} = 107 \pm 1$ kJ mol^{-1}, $\Delta^{\ddagger}H^{\theta} = 91 \pm 3$ kJ mol^{-1}, and $\Delta^{\ddagger}S^{\theta} = -53 \pm 8$ J K^{-1} mol^{-1}) for the subsequent thermal isomerization to stable (3*R*,3′*R*)-(*P*,*P*)-*trans*-**3**.[43] From these data, the half-life of the unstable

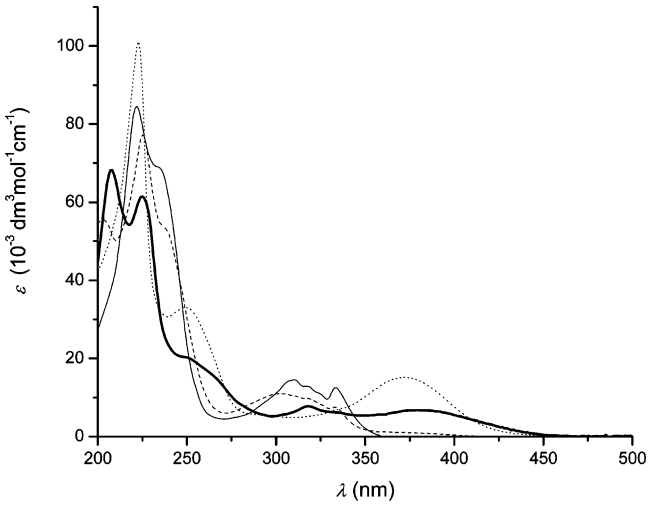

Figure 14. UV−vis spectra (*n*-hexane) observed during the rotary cycle of **3**: (3*R*,3′*R*)-(*P*,*P*)-*trans*-**3** (thin solid); (3*R*,3′*R*)-(*M*,*M*)-*cis*-**3** (thick solid); (3*R*,3′*R*)-(*P*,*P*)-*cis*-**3** (dashed); (3*R*,3′*R*)-(*M*,*M*)-*trans*-**3** (dotted).

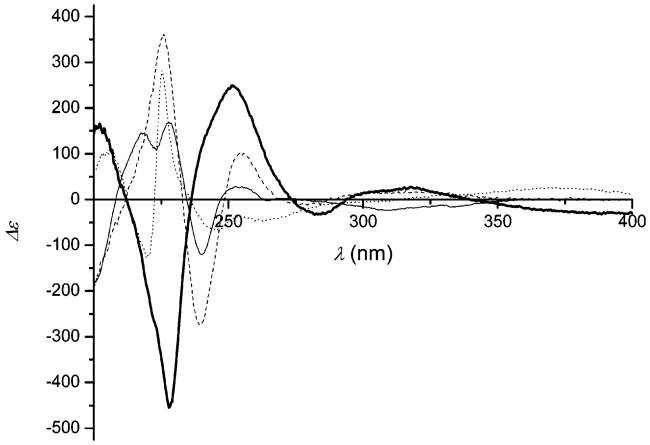

Figure 15. CD spectra (*n*-hexane) observed during the rotary cycle of **3**: (3*R*,3′*R*)-(*P*,*P*)-*trans*-**3** (thin solid); (3*R*,3′*R*)-(*M*,*M*)-*cis*-**3** (thick solid); (3*R*,3′*R*)-(*P*,*P*)-*cis*-**3** (dashed); (3*R*,3′*R*)-(*M*,*M*)-*trans*-**3** (dotted).

(43) The photochemical properties of (3*S*,3′*S*)-(*M*,*M*)-*cis*-**2** and (3*R*,3′*R*)-(*P*,*P*)-*cis*-**3** are expected to be identical in dodecane and *n*-hexane. The higher boiling point of dodecane (180 °C) is, however, suitable to determine the rate of the thermal helix inversion.

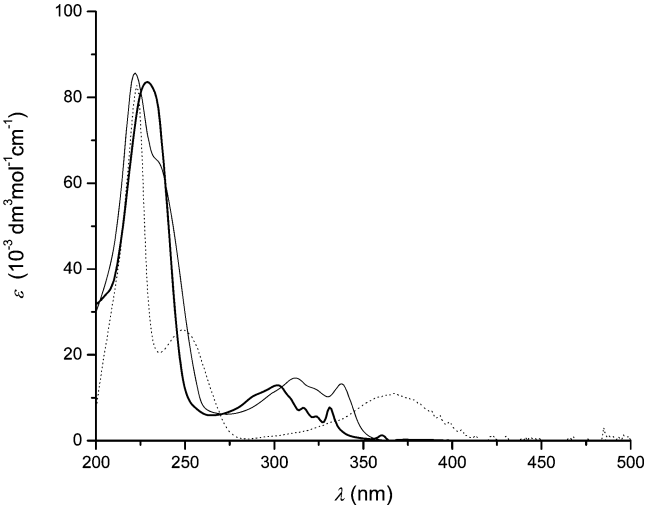

Figure 16. UV−vis spectra of all three *trans*-isomers of **4**: (3*S**,3′*S**)-(*P**,*P**)-*trans*-**4** (solid line); (3*S**,3′*S**)-(*M**,*M**)-*trans*-**4** (dotted line); (3*S**,3′*S**)-(*P**,*M**)-*trans*-**4** (thick solid line).

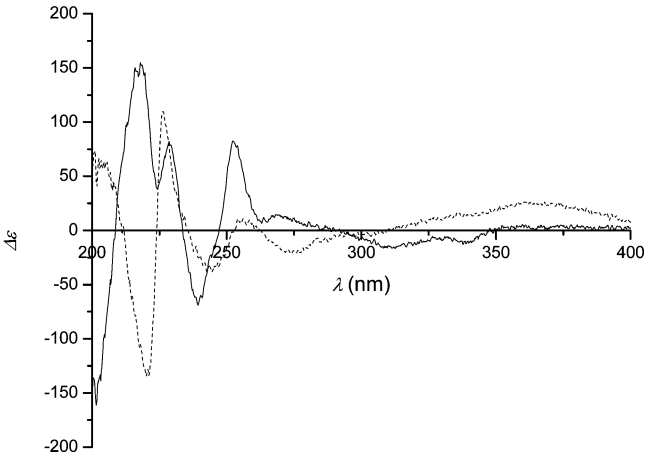

Figure 17. CD spectra for (3*S*,3′*S*)-(*P*,*P*)-*trans*-**4** (solid) and (3*S*,3′*S*)-(*M*,*M*)-*trans*-**4** (dotted) in *n*-hexane.

trans-**3** isomer was calculated to be 317 h at room temperature ($T = 293.15$ K).

Photochemical and Thermal Behavior of the *i*-Propyl Substituted Molecular Motor. The photochemical and thermal behavior of the *i*-propyl substituted molecular motor **4** is remarkably different from that of motors **2** and **3**. The enantiomers of the *i*-propyl substituted motor molecule **4** could be resolved by preparative chiral HPLC (Chiralpack OD, *n*-hexane:*i*-propanol = 99.9:0.1). The UV−vis spectrum (Figure 16) of (3*S*,3′*S*)-(*P*,*P*)-*trans*-**4** is similar to that of the motor molecules **2** and **3**. The shape and intensity of the CD spectrum of (3*S*,3′*S*)-(*P*,*P*)-*trans*-**4**, depicted in Figure 17, closely resemble those of the (3*S*,3′*S*)-(*M*,*M*)-*trans*-**2** and (3*R*,3′*R*)-(*P*,*P*)-*trans*-**3**. By comparison of these three spectra, the first eluted fraction of the stable *trans*-**4** was assigned to be (3*S*,3′*S*)-(*P*,*P*)-*trans*-**4**. To perform a rotary cycle analogously to the other molecular motors, a solution of the stable (3*S*,3′*S*)-(*P*,*P*)-*trans*-**4** in *n*-hexane was irradiated at low temperature ($\lambda \geq 280$ nm, $T = -60$ °C). This resulted in a red shift in the UV−vis of the longest wavelength band from 320 to 370 nm (Figure 16). In the CD spectrum, the major absorption band at approximately 220 nm was largely inverted ($\Delta\epsilon = -134.2$).

Scheme 5. Observed Isomerization upon Irradiation of (3*S*,3′*S*)-(*P*,*P*)-*trans*-**4**

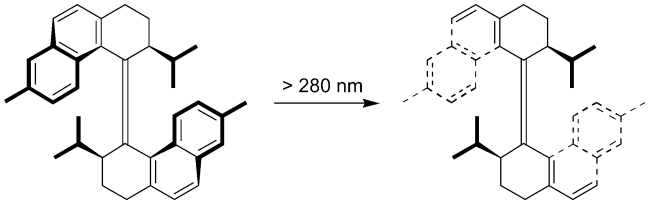

HPLC analysis indicated that the stable (3*S*,3′*S*)-(*P*,*P*)-*trans*-**4** had been completely converted to a new isomer. Upon heating at 60 °C or subsequent irradiation with light of different wavelengths ($\lambda = 256$, 313, 343, and 436 nm or $\lambda \geq 280$ nm), no change in UV−vis or CD signals could be observed. On the basis of comparison with data obtained for molecular motors **2** and **3**, the UV−vis and CD suggested that irradiation of stable (3*S*,3′*S*)-(*P*,*P*)-*trans*-**4** led directly to (3*S*,3′*S*)-(*M*,*M*)-*trans*-**4** (Scheme 5), because the observed spectra closely resemble that of the unstable *trans*-isomers of both **2** and **3**.

This is also the reason that (3*S*,3′*S*)-(*M*,*M*)-*cis*-**4** could not be formed by irradiation of (3*S*,3′*S*)-(*P*,*P*)-*trans*-**4**. Extensive ^{1}H NMR studies were performed to establish that the structure of the new isomer was correctly assigned as (3*S*,3′*S*)-(*M*,*M*)-*trans*-**4**.[44] Irradiation of stable (3*S**,3′*S**)-(*P**,*P**)-*trans*-**4** in both benzene-d_6 and toluene-d_8 gave complete conversion to the new isomer of *trans*-**4**. Judging from the ^{1}H NMR spectra, and especially the absorptions between δ 8.0 and 9.0 ppm, it was concluded that the new isomer had indeed a *trans*-geometry. A *cis*-geometry could be excluded, because protons of *cis*-isomers of these overcrowded alkenes generally have absorptions between δ 6.0 and 7.0 ppm. Light yellow, block-shaped crystals of the unstable (3*S**,3′*S**)-(*M**,*M**)-*trans*-**4**[35,45] suitable for X-ray analysis were obtained by recrystallization from heptane. It was difficult to obtain reliable data from these crystals. Measurement of the crystals at low temperature (100 K) failed. Although the X-ray structure determination at room temperature was thwarted by multiple reflection spots, a structure was found that fitted the experimental data. These results show that the structure had correctly been assigned as (3*S**,3′*S**)-(*M**,*M**)-*trans*-**4** (Figure 18). This new *trans*-isomer of **4** was found to be pseudo-C_2-symmetric, because small deviations in the solid state are found as compared to the ideal C_2-symmetry in solution. The substituents are in the (pseudo-)equatorial, unstable orientation. As a consequence, the naphthalene moiety and the *i*-propyl substituent are on opposite sides with respect to the central double bond. In contrast to the structures of the stable *trans*-isomers of **2**, **3**, and **4**, the central double bond is elongated (1.366 Å) and twisted to a considerable extent as is obvious from the Newman projection depicted in Figure 18. A similar twist in the alkene moiety was found for the structure of the unstable *trans*-isomer of **1**.[46] This twist might account for the yellow color of the compound in which a partial polarization over the central double bond has taken place.[47]

(44) Because irradiation of solutions of these alkenes in $CDCl_3$ frequently leads to significant product decomposition and formation of numerous side-products, experiments were performed in benzene-d_6 and toluene-d_8.
(45) Throughout this paper, (3*S**,3′*S**)-(*M**,*M**)-*trans*-**4** and (3*R**,3′*R**)-(*P**,*P**)-*trans*-**4** are referred to as unstable isomers. However, this *trans*-isomer of **4** is stable at room temperature and is converted to the other *trans*-isomers only at elevated temperatures.
(46) Koumura, N.; Harada, N. *Chem. Lett.* **1998**, 1151−1152.

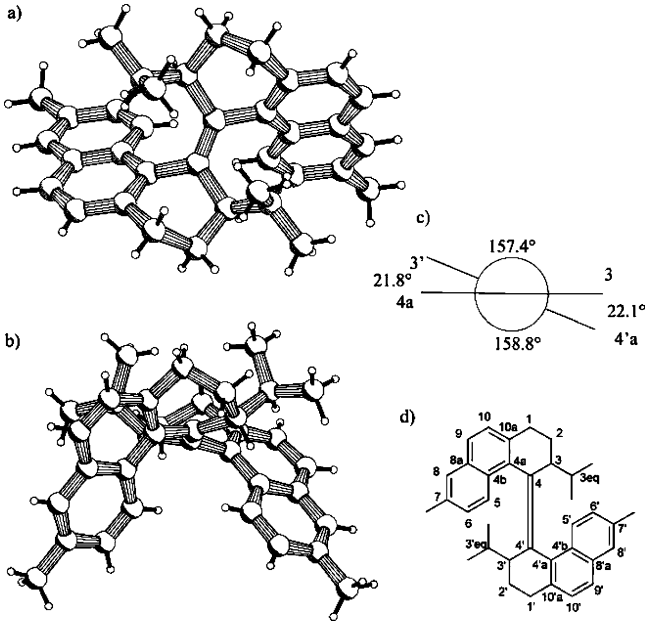

Figure 18. Pluto drawings of the unstable (3*R**,3′*R**)-(*P**,*P**)-*trans*-**4** seen perpendicular (a) and along the central double bond (b). The structure does not express the absolute stereochemistry of the molecule. Newman projection of the configuration around the central double bond viewed along the $C_4-C_{4'}$ axis (c) and the numbering scheme employed for the molecule (d).

Although it appeared that upon irradiation direct conversion of (3*S*,3′*S*)-(*P*,*P*)-*trans*-**4** to (3*S*,3′*S*)-(*M*,*M*)-*trans*-**4** occurred, more detailed investigations following the fluorescence of both isomers ($\lambda_{ex} = 344$ nm) revealed that the conversion is not a first-order process and that intermediate structures are involved. These measurements could be performed readily due to the distinct difference in emission wavelengths of (3*S*,3′*S*)-(*P*,*P*)-*trans*-**4** ($\lambda_{em} = 374$ nm) and (3*S*,3′*S*)-(*M*,*M*)-*trans*-**4** ($\lambda_{em} = 568$ nm) using the same wavelength of excitation ($\lambda_{ex} = 344$ nm).[35] This outcome of the photochemical reaction contrasts with the behavior observed for both (3*S*,3′*S*)-(*M*,*M*)-*trans*-**2** and (3*R*,3′*R*)-(*P*,*P*)-*trans*-**3**.

Although the new isomer (3*S*,3′*S*)-(*M*,*M*)-*trans*-**4** was stable at room temperature, it was demonstrated by CD measurements performed in dodecane that (3*S*, 3′*S*)-(*M*,*M*)-*trans*-**4** was converted slowly to (3*S*,3′*S*)-(*P*,*P*)-*trans*-**4** at elevated temperatures ($T = 110$ °C).

The isomerization processes were also investigated by ^{1}H NMR. A sample of stable (3*S**,3′*S**)-(*P**,*P**)-*trans*-**4** in toluene-d_8 was irradiated ($\lambda \geq 280$ nm, $T = 20$ °C), which resulted in full conversion to (3*S**,3′*S**)-(*M**,*M**)-*trans*-**4**. Carefully monitoring the sample by ^{1}H NMR during irradiation showed that during the initial 30 min of the irradiation a small amount of another isomer was formed, clearly distinct from the (3*S**,3′*S**)-(*P**,*P**)-*trans*-**4** and (3*S**,3′*S**)-(*M**,*M**)-*trans*-**4** isomers. This new isomer had not been seen while performing the UV−vis and CD experiments, which is due to the very small amount (<1%) of the isomer formed during the photochemical experiments. Aromatic absorptions originating from this new isomer appeared in the ^{1}H NMR as low as δ 6.6 ppm, and other new signals were identified at δ 0.80−0.81 (d) and 1.01−1.02 (d) and 1.96 (s) ppm. These signals were tentatively assigned as originating from a *cis*-isomer of **4**. Attempts to isolate this new isomer failed due to the very small amounts formed. This new isomer is, however, a thermally stable compound, because prolonged heating did not lead to conversion to the stable (3*S**,3′*S**)-(*P**,*P**)-*trans*-**4** or another isomer. Upon prolonged irradition for 2 h of the sample, all of the presumed *cis*-isomer of **4** was completely converted to (3*S**,3′*S**)-(*M**,*M**)-*trans*-**4**. The sample was then heated ($T = 110$ °C), and the decay in the signals of the unstable (3*S**,3′*S**)-(*M**,*M**)-*trans*-**4** was monitored. Surprisingly, during heating, signals belonging to yet another isomer appeared.

The isomerization process is therefore not a simple unimolecular process. The sample used for the ^{1}H NMR experiment contained three isomers of *trans*-**4**, and there was significant overlap with the absorption of the toluene-d_8 in the aromatic region, which complicated the interpretation of the spectrum. However, the most interesting absorptions originating from the methyl groups at C_7 and $C_{7'}$, the proton signals of H_5 and $H_{5'}$, and from the methyl groups of the *i*-propyl at the stereogenic center could be observed separately. For the stable (3*S**,3′*S**)-(*P**,*P**)-*trans*-**4**, these doublet signals can be found at δ 0.42−0.44, 0.97−0.99, and 8.72−8.74. After irradiation, these doublets have shifted to δ 0.19−0.21, 0.74−0.76, and 8.60−8.62 ppm and were assigned to (3*S**,3′*S**)-(*M**,*M**)-*trans*-**4**. Heating of the less stable (3*S**,3′*S**)-(*M**,*M**)-*trans*-**4** gave rise to a doubling of the absorptions in the entire spectrum relative to the number of absorptions of (3*S**,3′*S**)-(*M**,*M**)-*trans*-**4** or (3*S**,3′*S**)-(*P**,*P**)-*trans*-**4**. Interestingly, the new absorptions in the spectrum appear to be pairs having the same integration. This is clearly seen from Figure 19, where the absorptions originating from H_5 and $H_{5'}$ are shown during the thermal interconversion process. These data suggested that these absorptions originated from a single isomer of **4**, which is no longer C_2-symmetric. Most striking is that the original three doublet signals seem to have split into three pairs of two absorptions at δ 0.29−0.30, 0.32−0.34, 0.50−0.51, 0.67, 8.27−8.29, and 8.53−8.55 ppm, of which all are doublets except the broad singlet signal at 0.67 ppm. Upon continued heating, the intensity of the new absorptions gradually decreased and the signals of the original stable (3*S**,3′*S**)-(*P**,*P**)-*trans*-**4** reappeared slowly (Figure 19). Decisive evidence for the structure of this intermediate form in the thermal helix inversion of (3*S**,3′*S**)-(*M**,*M**)-*trans*-**4** to (3*S**,3′*S**)-(*P**,*P**)-*trans*-**4** was obtained by X-ray analysis.[35] This intermediate form turns out to be a *meso*-like isomer: (3*S**,3′*S**)-(*P**,*M**)-*trans*-**4**. In the absence of the stereogenic centers, this isomer would be a *meso*-compound and hence not chiral.[48] The orientation of the *i*-propyl substituents can clearly be distinguished (Figure 20); one of the *i*-propyl substituents has a (pseudo-)axial orientation, and the other has a (pseudo-)equatorial orientation. One of the substituents is therefore on the same side as the naphthalene with respect to the central double bond; the other one is not. Remarkable is that the central double bond, which is not elongated to a large extent (1.344 Å), shows only significant deviation from planarity at the side where the *i*-propyl substituent has a (pseudo-)-equatorial orientation. (3*S**,3′*S**)-(*P**,*M**)-**4** is C_1-symmetric, which accounts for the fact that the signals observed in the ^{1}H

(47) Sandström, J. *Top. Stereochem.* **1983**, *14*, 83−181.

(48) For numbering convenience, the carbon atom of the double bond in the half of the molecule with the (3*S**)-(*P**) relative chirality is arbitrarily assigned to be C_4. The other carbon atom of the double bond in the half with the relative (3*S**)-(*M**) stereochemistry is arbitrarily assigned to be $C_{4'}$.

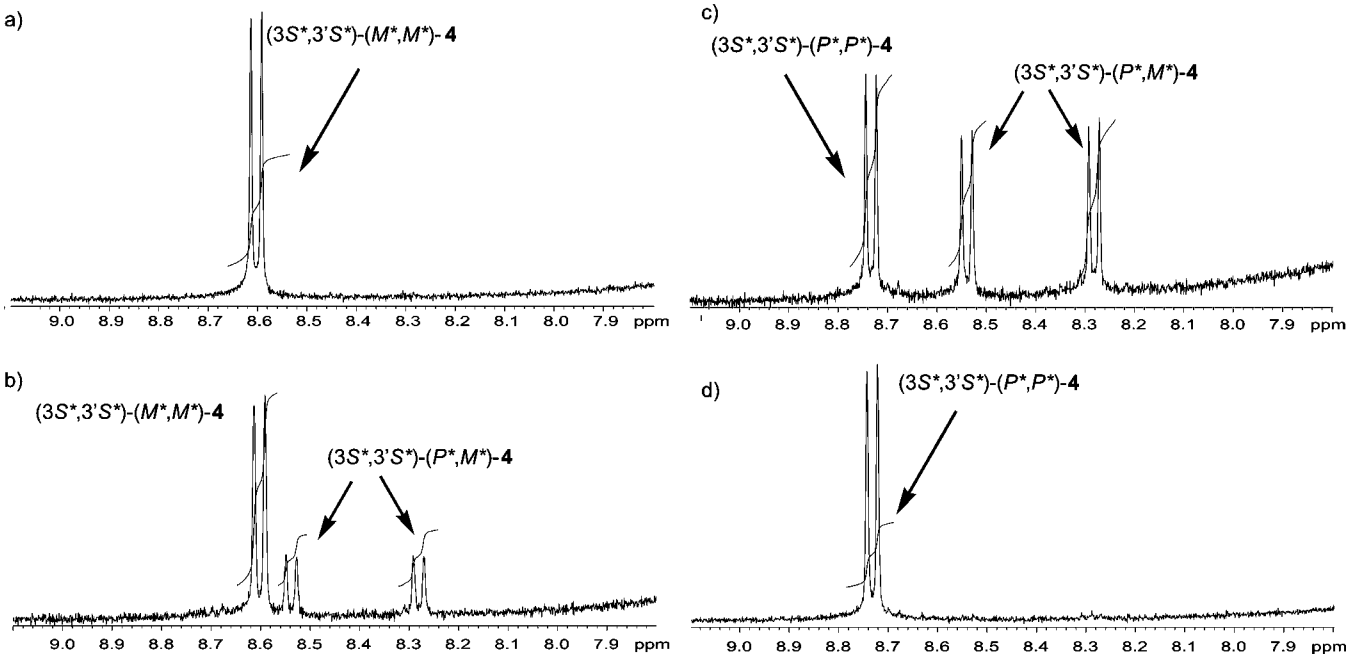

Figure 19. Conversion in time at $T = 110$ °C (chronologically from spectrum (a) $t = 0$; (b) $t = 0.85$ h; (c) $t = 6.0$ h; (d) after 30 d) of the unstable (3*S**,3′*S**)-(*M**,*M**)-*trans*-**4** via the (3*S**,3′*S**)-(*P**,*M**)-*trans*-**4** to (3*S**,3′*S**)-(*P**,*P**)-*trans*-**4** measured by ^{1}H NMR in toluene-d_8.

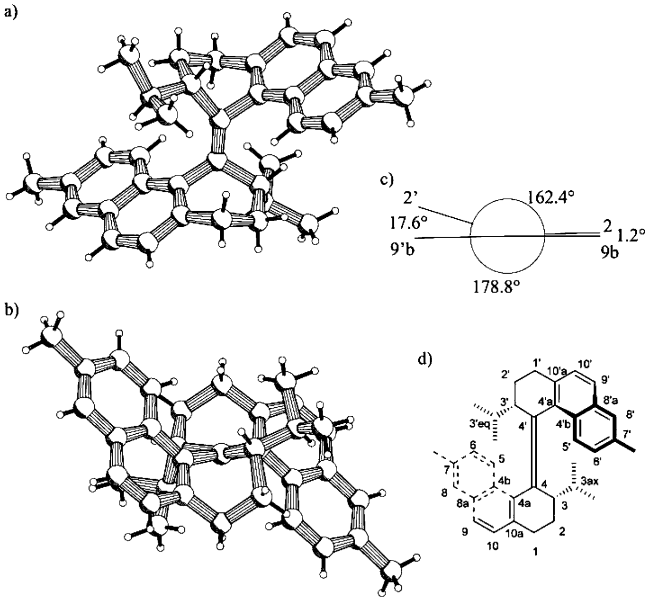

Figure 20. Pluto drawings of (3*S**,3′*S**)-(*P**,*M**)-*trans*-**4** as seen perpendicular (a) or along the central double bond (b). The Newman projection (c) and the numbering scheme (d) adopted for the molecule are also depicted.

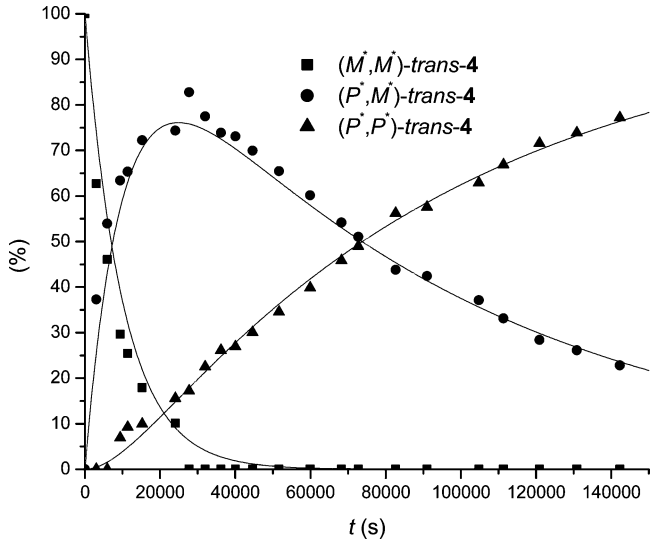

Figure 21. Conversion followed in time by ^{1}H NMR in toluene-d_8 ($T = 110$ °C) from (3*S**,3′*S**)-(*M**,*M**)-*trans* via (3*S**,3′*S**)-(*P**,*M**)-*trans* to (3*S**,3′*S**)-(*P**,*P**)-*trans*-**4**.

NMR have doubled as compared to those of the C_2-symmetric (3*S**,3′*S**)-(*M**,*M**)-*trans*-**4** and (3*S**,3′*S**)-(*P**,*P**)-*trans*-**4** isomers.

This demonstrates that the conversion of (3*S**,3′*S**)-(*M**,*M**)-*trans*-**4** to (3*S**,3′*S**)-(*P**,*P**)-*trans*-**4** is not a single step process. The first thermal helix inversion (of one-half of the molecule) going from (3*S**,3′*S**)-(*M**,*M**)-*trans*-**4** to (3*S**,3′*S**)-(*P**,*M**)-*trans*-**4** is relatively fast, while the second helix inversion going from (3*S**,3′*S**)-(*P**,*M**)-*trans*-**4** to (3*S**,3′*S**)-(*P**,*P**)-*trans*-**4** proceeds much slower. The entire process was followed in time ($T = 110$ °C) by ^{1}H NMR spectroscopy in toluene-d_8. The barrier for the first helix inversion obtained by a fitting procedure was $\Delta G^{\ddagger} = 124$ kJ mol^{-1} at $T = 383$ K, and for the second helix inversion using the same methodology, a value of $\Delta G^{\ddagger} = 131$ kJ mol^{-1} at $T = 383$ K was found (Figure 21).[35]

The UV−vis spectrum (Figure 16) of unstable (3*S**,3′*S**)-(*P**,*M**)-*trans*-**4** is very similar to that of stable (3*S**,3′*S**)-(*P**,*P**)-*trans*-**4**, as only a slight blue shift has taken place. Because (3*S**,3′*S**)-(*P**,*M**)-*trans*-**4** is nearly a *meso*-compound, it would be interesting to obtain a CD spectrum. It is expected that the Cotton effects for this compound would be relatively small. However, all attempts to resolve (3*S**,3′*S**)-(*P**,*M**)-*trans*-**4** into its enantiomers by chiral HPLC have so far been unsuccessful.

Discussion

The results for biphenanthrylidenes **2** and **3** clearly show that these molecules are molecular motors; that is, they are capable

Scheme 6. Rotary Scheme of Molecular Motor **4**

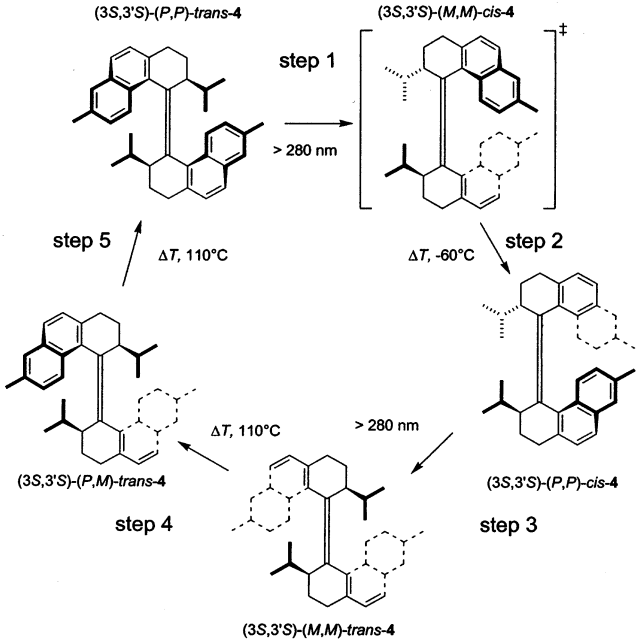

of a 360° unidirectional rotation around their central double bond. Kinetic measurements revealed that the increased steric hindrance in the ethyl substituted molecular motor **3** led to an increased rate of both thermal helix inversions. This small, but significant, effect might be caused by a destabilization of the ground state of ethyl-**3** as compared to methyl-**2**, and hence to a lowering of the activation energy. It was expected that *i*-propyl-**4** would follow this trend, but it is clear from the data presented that the properties of *i*-propyl substituted molecule **4** differ significantly from the methyl and ethyl substituted molecular motors **2** and **3**. The anticipated isomerization pathways starting with (3*S*,3′*S*)-(*P*,*P*)-*trans*-**4** are shown in Scheme 6. During irradiation experiments, evidence was found for the existence of (3*S**,3′*S**)-(*P**,*P**)-*cis*-**4**. Unfortunately, unequivocal structure assignment is prevented because only small amounts of the *cis*-isomer **4** are formed. After the formation of the *cis*-isomer of **4**, a second photochemical reaction takes place to form (3*S**,3′*S**)-(*M**,*M**)-*trans*-**4**. The presence of (3*S**,3′*S**)-(*P**,*P**)-*cis*-**4** in the isomerization cycle offers an acceptable explanation for the observed behavior of the alkene, because such behavior was never observed for other related biphenanthrylidenes. Also, so far we have never observed for these molecules photochemical isomerizations that convert one *trans*-isomer to another. Therefore, the alternative, direct photoexcitation of (3*S**,3′*S**)-(*P**,*P**)-*trans*-**4** to (3*S**,3′*S**)-(*M**,*M**)-*trans*-**4** offers a less likely explanation for the observed behavior. The fluorescence measurements also confirm the presence of an intermediate structure in the photochemical conversion of stable (3*S**,3′*S**)-(*P**,*P**)-*trans*-**4** to unstable (3*S**,3′*S**)-(*M**,*M**)-*trans*-**4**. In view of the fact that all photoisomerizations of this class of olefins have resulted in trans−cis isomerization, so far, the appearance of an isomer as evident from ^{1}H NMR and fluorescence and the clean photochemical process, it is safe to assign a (3*S**,3′*S**)-(*P**,*P**)-*cis*-**4** structure to this isomer.

Therefore, it is proposed that in the first photochemical step, the stable (3*S**,3′*S**)-(*P**,*P**)-*trans*-**4** is converted to the unstable (3*S**,3′*S**)-(*M**,*M**)-*cis*-**4** isomer (Scheme 6). This compound is highly unstable due to severe steric hindrance, and as a consequence a thermal helix inversion takes place almost instantaneously at temperatures as low as −60 °C to form the observable stable (3*S**,3′*S**)-(*P**,*P**)-*cis*-**4**. Upon continued irradiation of (3*S**,3′*S**)-(*P**,*P**)-*cis*-**4** at the same wavelength, (3*S**,3′*S**)-(*M**,*M**)-*trans*-**4** is formed, and, due to the very favorable photoequilibrium between the former two compounds, the equilibrium is shifted completely to (3*S**,3′*S**)-(*M**,*M**)-*trans*-**4**, which is stable at ambient temperatures. The thermal helix inversion of this compound takes place in two steps, involving (3*S**,3′*S**)-(*P**,*M**)-*trans*-**4** as an intermediate as was proven by ^{1}H NMR and X-ray analysis. We have already predicted the interconversion between a molecule with a (*P*,*P*)-helical structure and a molecule with a (*M*,*M*)-helical structure, based on extensive calculation, to proceed through an intermediate structure with a (*P*,*M*)-helical structure.[49] Due to steric crowding, the energy barrier for both processes in the *i*-propyl substituted alkene described here has been increased to such an extent that in the two-step process the intermediate isomer could be identified. In conclusion, it is evident that **4** still behaves like a molecular motor (Scheme 6). Experimental proof for each step in the rotary cycle is, however, hard to obtain due to the instability of the (3*S**,3′*S**)-(*M**,*M**)-*cis*-**4** and the complete photochemical conversion of (3*S**,3′*S**)-(*P**,*P**)-*cis*-**4** to (3*S**,3′*S**)-(*M**,*M**)-*trans*-**4**. Although alkene **4** is not particularly interesting as a motor molecule, due to the very slow thermal isomerization it offers detailed insight in the thermal helix isomerization step going from unstable *trans*-**4** to stable *trans*-**4**. The key observation is that the thermal isomerization is a two-step process with two consecutive helix inversions. This stepwise isomerization process has never been demonstrated experimentally for any other overcrowded alkene, and this study offers therefore more detailed insights into the rotary behavior of these motor molecules.

Conclusion

The thermal and photochemical behavior of new first generation molecular motors has been the main subject of this paper. Three new molecular motors **2**−**4** were synthesized with substituents of increasing size going from methyl to ethyl and finally *i*-propyl. The consequence of the increased steric bulk in the parent ketone is a decrease in the yield for the key McMurry reaction in which the severely hindered central double bond is formed. This low yield was not in all cases entirely due to the low reactivity of the ketone, but also due to the formation of structurally similar side products that were hard to separate from the desired alkene. All three molecular motors were synthesized in an eight-step synthetic sequence. Both the methyl and the ethyl substituted molecular motors **2** and **3** are able to perform a unidirectional rotation around their central double bonds in a four-stage process involving two photochemical and two thermal isomerization steps. The differences between these two motor molecules were found to be rather small. The ethyl molecular motor **3** has a slightly higher speed of rotation than the methyl substituted analogue, which may be attributed to the slightly increased instability of the isomers with equatorial

(49) Zijlstra, R. W. J.; Jager, W. F.; de Lange, B.; van Duijnen, P. Th.; Feringa, B. L.; Goto, H.; Saito, A.; Koumura, N.; Harada, N. *J. Org. Chem.* **1999**, *64*, 1667−1674.

substituents. Although also the *i*-propyl substituted molecular motor is able to perform a unidirectional rotation, not all four isomers usually observed could be detected experimentally. The thermal isomerization of the unstable *trans*-**4** to the stable *trans*-**4** is very slow. This allowed the observation of an intermediate, *meso*-like form of *trans*-**4**, which demonstrates for the first time that the thermal helix inversion is a stepwise process involving two consecutive helix inversions.

Experimental Section

General. The high-resolution one- and two-dimensional ^{1}H NMR spectra were obtained using a Varian Gemini-200, Varian VXR-300, Varian Mercury Plus, and a Varian Unity Plus Varian-500 operating at 199.97, 299.97, 399.93, and 499.86 MHz, respectively, for the ^{1}H nucleus. ^{13}C NMR spectra were recorded on a Varian Gemini-200, Varian VXR-300, Varian Mercury Plus, and a Varian Unity Plus Varian-500 operating at 50.29, 75.43, 100.57, and 125.70 MHz, respectively. Chemical shifts are reported in δ units (ppm) relative to the residual deuterated solvent signals of $CHCl_3$ (^{1}H NMR, δ 7.26 ppm; ^{13}C NMR, δ 77.0 ppm), benzene (^{1}H NMR, δ 7.15 ppm; ^{13}C NMR, δ 128.0 ppm), and toluene (^{1}H NMR, δ 2.08 ppm). The splitting patterns are designated as follows: s (singlet), d (doublet), t (triplet), q (quartet), m (multiplet), and br (broad). Melting points were taken on a Mettler FP-2 melting point apparatus, equipped with a Mettler FP-21 microscope. Optical rotations were measured with a Perkin-Elmer 241 polarimeter. UV−vis measurements were performed on a Hewlett-Packard HP 8453 FT spectrophotometer, and CD spectra were recorded on a JASCO J-715 spectropolarimeter using Uvasol grade solvents (Merck). MS (EI) and HRMS (EI) spectra were obtained with a JEOL JMS-600 spectrometer. Elemental analyses were performed in the microanalytical department with a Foss-Heraeus CHN-O-Rapid or a EuroVector Euro EA Elemental Analyzer. The average values of duplo measurements are reported. Column chromatography was performed on silica gel (Aldrich 60, 230−400 mesh). HPLC analyses were performed on Shimadzu HPLC system equipped with two LC-10AD*vp* solvent delivery systems, a DGU-14A degasser, a SIL-10AD*vp* autosampler, a SPD-M10A UV/vis photodiode array detector, a CTO-10A*vp* column oven, and a SCL-10A*vp* controller unit using Chiralcel OD (Daicel), Chiralcel AD (Daicel), (*R*,*R*)-Whelk 01 (Regis), and Chiralcel OB-H (Daicel) columns. Preparative HPLC was performed on a Gilson HPLC system consisting of a 231XL sampling injector, a 306 (10SC) pump, an 811C dynamic mixer, a 805 manometric module, with a 119 UV/vis detector and a 202 fraction collector, using the Chiralcel OD (Daicel) column. The elution speed was 1 mL min^{-1}. Solvents were distilled and dried before use by standard methodology. Chemicals were used as received from Acros, Aldrich, Fluka, or Merck. Irradiation experiments were performed with a 180 W Oriel Hg-lamp using a Pyrex filter or filters of the appropriate wavelengths. Photostationary states were ensured by monitoring composition changes in time by taking UV−vis spectra at distinct intervals until no changes were observed. Thermal helix inversions were monitored by CD spectroscopy using the apparatus described above and a JASCO PFD-350S/350L Peltier type FDCD attachment with a temperature control.

(3*S*,3′*S*)-(*M*,*M*)-*trans*-(+)-1,1′,2,2′,3,3′,4,4′-Octahydro-3,3′,7,7′-tetramethyl-4,4′-biphenanthrylidene (2). The racemic (3*R**,3′*R**)-(*P**,*P**)-*trans*-(±)-**2** was prepared according to the procedure below for *trans*-**3**. The reaction was performed with ketone **7** (600 mg, 2.7 mmol) and yielded after the reaction and purification racemic **2** as a white solid (50 mg, 0.12 mmol, 9.0%); ^{1}H NMR (300 MHz, $CDCl_3$) δ 0.77−0.79 (d, J = 7.0 Hz, 6H), 1.21−1.31 (dtd, J = 13.2, 7.0, 3.3 Hz, 2H), 1.82−1.93 (m, 2H), 2.55 (s, 6H), 2.63−2.68 (dtd, J = 13.2, 7.0, 3.3 Hz, 2H), 2.67−2.70 (d, J = 7.0 Hz, 4H), 7.26−7.29 (m, 2H), 7.37−7.40 (dd, J = 1.8, 8.8 Hz, 2H), 7.64−7.67 (d, J = 8.4 Hz, 2H), 7.65 (s, 2H), 8.31−8.34 (d, J = 8.8 Hz, 2H); ^{13}C NMR (75 MHz, $CDCl_3$) δ 18.5 (q), 21.1 (q), 27.3 (t), 31.2 (t), 33.8 (d), 125.7 (d), 125.8 (d), 126.6 (d), 127.2 (d), 127.9 (d), 130.6 (s), 132.4 (s), 134.1 (s), 134.6 (s), 135.5 (s), 136.3 (s); *m*/*z* (EI, %) = 418 (6), 417 (35), 416 (M^+, 100), 401 (12), 359 (10); HRMS (EI) calcd for $C_{32}H_{32}$, 416.2504; found, 416.25172. Anal. Calcd (%): C, 92.46; H, 7.74. Found (%): C, 91.94; H, 7.82. UV−vis and CD spectroscopic data for pure (3*S*,3′*S*)-(*M*,*M*)-*trans*-**2**: UV−vis (*n*-hexane) λ_{max} (ϵ) 221 (83 500), 223 (67 400), 310 (14 800), 333 (13 300); CD (*n*-hexane) λ_{max} ($\Delta\epsilon$) 218.2 (−128.5), 222.8 (−83.8), 228.8 (−167.0), 240.0 (+97.4), 256.4 (−21.7), 265.0 (+8.4), 272.0 (−1.0), 309.4 (+22.3). UV−vis and CD spectroscopic data observed during the rotary cycle for (3*S*,3′*S*)-(*P*,*P*)-*cis*-**2**: UV−vis (*n*-hexane) λ_{max} (ϵ) 207 (68 500), 226 (63 300), 317 (8900); CD (*n*-hexane) λ_{max} ($\Delta\epsilon$) 227.2 (+470.5), 251.0 (−195.5), 272.6 (+32.1), 304.4 (−14.4), 362.8 (+30.3). (3*S*,3*S*′)-(*M*,*M*)-*cis*-**2**: UV−vis (*n*-hexane) λ_{max} (ϵ) 226 (77 400), 238 (54 800), 301 (13 700); CD (*n*-hexane) λ_{max} ($\Delta\epsilon$) 225.4 (−367.5), 240.2 (+264.3), 255.4 (−114.1), 279.0 (+11.0), 329.4 (−20.6). (3*S*,3′*S*)-(*P*,*P*)-*trans*-**2**: UV−vis (*n*-hexane) λ_{max} (ϵ) 222 (100 900), 367 (15 300); CD (*n*-hexane) λ_{max} ($\Delta\epsilon$) 219.4 (+151.0), 224.8 (−247.4), 244.0 (+43.1), 369.8 (−28.8). For analytical purposes, the resolution of *trans*-**2** was performed by chiral HPLC using a Daicel Chiralcel OD column as the stationary phase and a mixture of heptane:*i*-propanol in a ratio of 99:1 as the eluent at a rate of 1 mL min^{-1}. The first eluted fraction (t = 3.90 min) of *trans*-**2** contained (3*S*,3′*S*)-(*M*,*M*)-*trans*-**2**, and the second fraction (t = 4.46 min) contained (3*R*,3′*R*)-(*P*,*P*)-*trans*-**2**. The enantiomers of *trans*-**2** can be separated also with a mixture of heptane:*i*-propanol in a ratio of 99.5:0.5 as the eluent (first fraction t = 4.75 min; second fraction t= 6.23 min).

(3*S*,3′*S*)-(*M*,*M*)-*cis*-(+)-1,1′,2,2′,3,3′,4,4′-Octahydro-3,3′,7,7′-tetramethyl-4,4′-biphenanthrylidene (2). Irradiation of a saturated solution of the enantiomerically pure (3*S*,3′*S*)-(*M*,*M*)-*trans*-**2** in *n*-hexane at −65 °C overnight and subsequent heating at 60 °C during 4 h gave a mixture of two isomeric compounds. These two isomers were separated by preparative HPLC using a Daicel Chiralcel OD column as the stationary phase and a mixture of heptane:*i*-propanol = 99.5:0.5 as the eluent. The fraction collected with a retention time of t = 6.00 min contained the desired (3*S*,3′*S*)-(*M*,*M*)-*cis*-**2**, and this material was obtained as a white solid with the following physical properties: ^{1}H (300 MHz, $CDCl_3$) δ 1.08−1.10 (d, J = 6.6 Hz, 6H), 1.17−1.26 (m, 2H), 2.16 (s, 6H), 2.46−2.53 (m, 2H), 2.81−2.85 (m, 4H), 3.56−3.63 (m, 2H), 6.51−6.54 (d, J = 7.3 Hz, 2H), 6.87−6.90 (d, J = 8.4 Hz, 2H), 7.00 (s, 2H), 7.10−7.18 (m, 4H); ^{13}C (75 MHz, $CDCl_3$) δ 21.2 (q), 22.5 (q), 30.3 (t), 31.9 (t), 32.1 (d), 124.5 (d), 125.6 (d), 125.7 (d), 125.8 (d), 126.3 (d), 128.6 (s), 132.0 (s), 132.6 (s), 134.7 (s), 135.6 (s), 137.9 (s); UV−vis and CD spectroscopic data for pure (3*S*,3′*S*)-(*M*, *M*)-*cis*-**2**: UV−vis (*n*-hexane) λ_{max} (ϵ) 225 (80 100), 236 (55 300), 301 (11 400), 319 (10 600), 334 (8300); CD (*n*-hexane) λ_{max} ($\Delta\epsilon$) 225.6 (−407.9), 240.0 (311.6), 255.8 (−136.5), 280.6 (10.9), 326.4 (−21.6).

(3*S,3′*S**)-(*P**,*P**)-*trans*-(±)-1,1′,2,2′,3,3′,4,4′-Octahydro-3,3′,7,7′-tetramethyl-4,4′-biphenanthrylidene (2).** A solution of stable *cis*-**2** dissolved in hexane was irradiated for several hours at 0 °C. The hexane was then removed under reduced pressure at room temperature, and the slightly yellow solid was taken up in $CDCl_3$. The sample consisted of a mixture of stable *cis*-**2** and unstable *trans*-**2**. The absorptions of unstable *trans*-**2** were deduced by comparison with the ^{1}H NMR spectrum of pure stable *cis*-**2**; ^{1}H (300 MHz, $CDCl_3$) δ 0.31−0.33 (d, J = 6.6 Hz, 6H), 1.40−1.50 (m, 4H), 2.50 (s, 6H), 2.49−2.57 (m, 2H), 2.67−2.77 (m, 2H), 3.00−3.05 (m, 2H), 7.25−7.31 (m, 4H), 7.63 (s, 2H), 7.65−7.68 (d, J = 8.1 Hz, 2H), 8.47−8.49 (d, J = 8.8 Hz, 2H); ^{13}C (75 MHz, $CDCl_3$) δ 19.9 (q), 21.3 (q), 28.3 (t), 33.4 (t), 34.6 (d), 126.1 (d), 126.5 (d), 126.6 (d), 127.6 (d), 128.3 (d), 129.3 (s), 133.4 (s), 133.7 (s), 136.3 (s), 140.0 (s), 141.5 (s); UV−vis and CD spectroscopic data for pure (3*S*,3′*S*)-(*P*, *P*)-*trans*-**2**: UV−vis (*n*-hexane) λ_{max} (ϵ) 221 (100 700), 249 (36 900), 368 (17 500); CD (*n*-hexane) λ_{max} ($\Delta\epsilon$) 219.8 (179.1), 224.6 (−360.7), 243.8 (68.5), 253.4 (35.7), 262 (54.0), 376.0 (−37.4); the HPLC retention time of (3*S**,3′*S**)-(*P**,*P**)-

trans-**2** on a silica column as the stationary phase and using heptane as the eluent was 6.29 min.

(3*R,3′*R**)-(*P**,*P**)-*trans*-(±)-1,1′,2,2′,3,3′,4,4′-Octahydro-3,3′-diethyl-7,7′-dimethyl-4,4′-biphenanthrylidene (3).** A black slurry of zinc powder (4.16 g, 63.7 mmol) and $TiCl_4$ (3.5 mL, 6.0 g, 31.5 mmol) in the smallest amount of THF possible (15 mL) divided over four flasks was refluxed for 1 h. Because the McMurry reaction has frequently led to unpredictable results, the decision was made to perform the coupling in multiple small flasks. Over the cooled solutions was then divided by ratio of the amount of Zn/$TiCl_4$ the ketone **13** (3.81 g, 16.0 mmol) in a small amount of THF (10 mL). The black slurry was then refluxed for 1 week. The reaction mixtures were poured into a saturated aqueous solution of NH_4Cl (400 mL) and extracted with ethyl acetate (2 × 250 mL) and CH_2Cl_2 (3 × 250 mL). The combined organic layers were dried ($MgSO_4$), and the solvent was removed under reduced pressure to give a reddish tar. This tar was flushed over a silica column with pure hexane. Removal of the hexane under reduced pressure provided a yellow oil, which was taken up in a small amount of hexane. The yellowish crystals formed were thoroughly washed with hexane yielding a small amount of white crystals (257 mg, 7.2%); mp 237.6−238.2 °C; ^{1}H (300 MHz, $CDCl_3$) δ 0.51−0.56 (t, J = 7.3 Hz, 6H, $CH_{3,3ax}$), 0.71−0.85 (m, 2H, $CH_{2,3ax}$), 1.32−1.43 (m, 2H, H_2), 1.45−1.53 (m, 2H, $CH_{2,3ax}$), 1.68−1.79 (m, 2H, $H_{2'}$), 2.36−2.44 (m, 2H, H_{3eq}), 2.54 (s, 6H, Me_7), 2.68−2.72 (t, J = 7.3 Hz, 4H, H_1, $H_{1'}$), 7.25−7.28 (d, J = 7.7 Hz, 2H, H_{10}), 7.36−7.39 (d, J = 8.4 Hz, 2H, H_6), 7.63 (s, 2H, H_8), 7.63−7.66 (d, J = 7.7 Hz, 2H, H_9), 8.32−8.35 (d, J = 8.4 Hz, 2H, H_5); ^{13}C (75 MHz, $CDCl_3$) δ 12.0 (q), 21.5 (q), 26.5 (t), 27.4 (t), 27.5 (t), 40.5 (d), 125.6 (2 × d), 126.5 (d), 127.2 (d), 127.8 (d), 130.3 (s), 132.4 (s), 134.1 (s), 135.4 (s), 135.6 (s), 136.2 (s); *m*/*z* (EI, %) = 444 (M^+, 100); HRMS (EI) calcd for $C_{34}H_{36}$, 444.2817; found, 444.2816; Anal. Calcd (%): C, 91.84; H, 8.16. Found (%): C, 91.30; H, 8.28. UV−vis and CD spectroscopic data for pure (3*R*,3′*R*)-(*P*,*P*)-*trans*-**3**: UV−vis (*n*-hexane) λ_{max} (ϵ) 222 (84 600), 236 (68 100), 310 (14 500), 333 (12 500); CD (*n*-hexane) λ_{max} ($\Delta\epsilon$) 217.4 (+145.8), 223.2 (+108.1), 228.0 (+168.0), 240.2 (−119.7), 252.8 (+28.2), 309.4 (−23.8). UV−vis and CD spectroscopic data observed during the rotary cycle (3*R*,3′*R*)-(*M*,*M*)-*cis*-**3**: UV−vis (*n*-hexane) λ_{max} (ϵ) 208 (68 200), 225 (61 400), 318 (7700), 379 (6800); CD (*n*-hexane) λ_{max} ($\Delta\epsilon$) 227.8 (−455.2), 251.6 (+249.3), 282.0 (−32.8), 317.6 (+27.7), 397.0 (−31.7). (3*R*,3′*R*)-(*P*,*P*)-*cis*-**3**: UV−vis (*n*-hexane) λ_{max} (ϵ) 225 (77 300), 303 (11 000); CD (*n*-hexane) λ_{max} ($\Delta\epsilon$) 226.0 (+361.3), 239.4 (−274.1), 254.6 (+101.8), 279.2 (−12.0), 324.8 (+19.7). (3*R*,3′*R*)-(*M*,*M*)-*trans*-**3**: UV−vis (*n*-hexane) λ_{max} (ϵ) 223 (101 100), 249 (33 100), 371 (15 200); CD (*n*-hexane) λ_{max} ($\Delta\epsilon$) 219.6 (−127.5), 225.2 (+282.2), 244.8 (−66.1), 372.4 (+26.0). Resolution of racemic *trans*-**3** was performed by chiral HPLC using a Daicel Chiralcel OD column as the stationary phase and a mixture of heptane:*i*-propanol in a ratio of 99.9:0.1 as the eluent at a rate of 1 mL min^{-1}. The first eluted fraction (t = 6.44 min) contained (3*R*,3′*R*)-(*P*,*P*)-*trans*-**3**, and the second fraction (t = 10.20 min) contained (3*S*,3′*S*)-(*M*,*M*)-*trans*-**3**. For analytical purposes, the enantiomers of *trans*-**3** can be separated as well with a mixture of heptane:*i*-propanol in a ratio of 99.5:0.5 as the eluent (first fraction t = 4.04 min; second fraction t = 4.48 min).

(3*R,3′*R**)-(*P**,*P**)-*cis*-1,1′,2,2′,3,3′,4,4′-Octahydro-3,3′-diethyl-7,7′-dimethyl-4,4′-biphenanthrylidene (3).** A solution of *trans*-**3** in hexane was irradiated for 4 h at −40 °C. The solution was then heated for 4 h at 60 °C, and a mixture of (3*R**,3′*R**)-(*P**,*P**)-*trans*-**3** and (3*R**,3′*R**)-(*P**,*P**)-*cis*-**3** was obtained. These two isomers were separated by preparative HPLC using a silica column as the stationary phase and heptane as the eluent. The first eluted fraction (t = 4.94 min) contained (3*R**,3′*R**)-(*P**,*P**)-*trans*-**3**, and the second eluted fraction (t = 5.64 min) contained (3*R**,3′*R**)-(*P**,*P**)-*cis*-**3**; ^{1}H (300 MHz, $CDCl_3$) δ 0.94−0.99 (t, J = 7.5 Hz, 6H), 1.22−1.32 (m, 2H), 1.36−1.42 (m, 4H), 2.16 (s, 6H), 2.44−2.56 (m, 2H), 2.87−2.93 (m, 4H), 3.44−3.49 (m, 2H), 6.52−6.55 (d, J = 8.8 Hz, 2H), 6.94−6.97 (d, 8.8 Hz, 2H), 7.00 (s, 2H), 7.10−7.12 (d, J = 8.1 Hz, 2H), 7.16−7.18 (d, J = 8.1 Hz, 2H); ^{13}C (75 MHz, $CDCl_3$) δ 12.3 (q), 21.2 (q), 29.7 (t), 29.9 (t), 30.0 (t), 39.1 (t), 124.5 (d), 125.7 (2 × d), 125.9 (d), 126.2 (d), 128.4 (s), 132.0 (s), 132.5 (s), 135.5 (s), 135.6 (s), 137.2 (s); the enantiomers of *cis*-**3** can be separated using a Daicel Chiralcel OD column as the stationary phase and a mixture of heptane:*i*-propanol in a ratio of 99.5:0.5 as the eluent. The first fraction (t = 4.04 min) was assigned to be (3*R*,3′*R*)-(*P*,*P*)-*cis*-**3**, and the second fraction (t = 4.48 min) was assigned to be (3*S*,3′*S*)-(*M*,*M*)-*cis*-**3**.

(3*R,3′*R**)-(*M**,*M**)-*trans*-1,1′,2,2′,3,3′,4,4′-Octahydro-3,3′-diethyl-7,7′-dimethyl-4,4′-biphenanthrylidene (3).** A solution of stable *cis*-**3** dissolved in hexane was irradiated for several hours at 0 °C. The hexane was then removed under reduced pressure at room temperature, and the slightly yellow solid was taken up in $CDCl_3$. The sample consisted of a mixture of stable *cis*-**3** and unstable *trans*-**3**. The absorptions in the ^{1}H NMR were deduced by comparison of the ^{1}H NMR spectrum of pure stable *cis*-**3**. ^{1}H (300 MHz, $CDCl_3$) δ 0.02−0.07 (t, J = 7.3 Hz, 6H), 0.52−0.73 (m, 4H), 0.79−0.95 (m, 4H), 2.49−2.75 (m, 6H), 2.50 (s, 6H), 7.24−7.35 (m, 4H), 7.62−7.65 (m, 4H), 8.40−8.42 (d, J = 8.4 Hz, 2H); ^{13}C (75 MHz, $CDCl_3$) δ 12.5 (q), 21.3 (q), 26.1 (t), 28.4 (t), 28.8 (t), 42.4 (d), 126.2 (d), 126.5 (d), 126.9 (d), 127.5 (d), 128.3 (d), 129.0 (s), 133.6 (s), 133.6 (s), 136.0 (s), 139.0 (s), 140.9 (s); the HPLC retention time of (3*R**,3′*R**)-(*M**,*M**)-*trans*-**3** was 5.21 min using a silica column as the stationary phase and heptane as the eluent.

(3*S,3′*S**)-(*P**,*P**)-*trans*-1,1′,2,2′,3,3′,4,4′-Octahydro-3,3′-di-*i*-propyl-7,7′-dimethyl-4,4′-biphenanthrylidene (4).** Carefully $TiCl_4$ (1.6 mL, 14.6 mmol) was added by syringe to a suspension of zinc powder (1.9 g, 29.1 mmol) in THF (5 mL) cooled to 0 °C by an ice-bath. The resulting brown/black slurry was refluxed for 1.5 h. The ketone **14** (1.8 g, 7.1 mmol) was then added, and the mixture was heated at reflux for 10 d. The reaction mixture was poured into a saturated aqueous solution of NH_4Cl (200 mL) followed by extraction with ethyl acetate (3 × 200 mL). The combined organic layers were dried ($MgSO_4$), and all volatiles were removed under reduced pressure. The resulting brown oil was subjected to column chromatography. First, all apolar fractions were separated by flash column chromatography (SiO_2, heptane:ethyl acetate = 50:1) and were then further purified by column chromatography using pure heptane (SiO_2, heptane). The alkene **15**[35] (R_f = 0.54, 150 mg, 0.64 mmol, 8.9%) could be separated in this way from **4**, **16**,[35] and **17**[35] (R_f = 0.36). By repeated recrystallizations from heptane, the hydrocarbons **4**, **16**, and **17** could all be obtained pure: **4** (6.8 mg, 14.4 μmol, 0.41%), **16** (19.0 mg, 40.0 μmol, 1.13%), **17** (16.4 mg, 3.46 μmol, 0.97%); ^{1}H (300 MHz, $CDCl_3$) δ 0.45−0.48 (d, J = 6.6 Hz, 6H), 0.82−0.84 (d, J = 7.0 Hz, 6H), 1.32−1.42 (m, 2H), 1.55−1.72 (m, 4H), 2.25−2.32 (m, 2H), 2.55 (s, 6H), 2.68−2.88 (m, 4H), 7.19−7.22 (d, J = 8.4 Hz, 2H), 7.36−7.40 (dd, J = 8.4, 1.4 Hz, 2H), 7.60 (s, 2H), 7.60−7.62 (d, J = 8.4 Hz, 2H), 8.47−8.50 (d, J = 8.4 Hz, 2H); ^{1}H (300 MHz, C_6D_6) δ 0.44−0.46 (d, J = 6.6 Hz, 6H), 1.03−1.06 (d, J = 7.0 Hz, 6H), 1.53−1.71 (m, 6H), 2.30 (s, 6H), 2.55−2.66 (m, 4H), 2.74−2.83 (m, 2H), 7.15−7.17 (d, J = 8.4 Hz, 2H), 7.32−7.36 (dd, J = 8.6 Hz, 1.5 Hz, 2H), 7.49 (s, 2H), 7.56−7.59 (d, J = 8.4 Hz, 2H), 8.82−8.84 (d, J = 8.4 Hz, 2H); ^{1}H (400 MHz, C_7D_8) δ 0.42−0.44 (d, J = 6.6 Hz, 6H), 0.97−0.99 (d, J = 6.6 Hz, 6H), 1.33−1.69 (m, 6H), 2.31 (s, 6H), 2.49−2.54 (m, 2H), 2.57−2.65 (m, 2H), 2.75−2.82 (ddd, J = 17.2, 8.8, 4.4 Hz, 2H), 7.11−7.13 (d, J = 8.4 Hz, 2H), 7.27−7.30 (dd, J = 8.4, 1.5 Hz, 2H), 7.42 (s, 2H), 7.50−7.52 (d, J = 8.4 Hz, 2H), 8.72−8.74 (d, J = 8.4 Hz, 2H); ^{13}C (75 MHz, $CDCl_3$) δ 20.1 (q), 21.6 (q), 22.7 (q), 26.0 (t), 26.3 (t), 28.9 (d), 46.2 (d), 125.5 (d), 126.95 (d), 127.00 (d), 127.04 (d), 127.6 (d), 129.8 (s), 132.4 (s), 134.2 (s), 134.9 (s), 135.3 (s), 139.2 (s); *m*/*z* (EI, %) = 473 (41), 472 (M^+, 100), 429 (39), 359 (53); HRMS (EI) calcd for $C_{36}H_{40}$, 472.3130; found, 472.3134. Resolution of (3*S**,3′*S**)-(*P**,*P**)-*trans*-**4** was performed by chiral HPLC using a Chiralpack OD column as the stationary phase and a mixture of heptane:*i*-propanol in a ratio of 99.9:0.1 as the eluent at a rate of 1 mL min^{-1}. The first eluted fraction (t = 8.4 min) of *trans*-**4** contained (3*S*,3′*S*)-(*P*,*P*)-*trans*-**4**, and the second fraction (t

= *10.1 min) contained (3R,3′R)-(M,M)-trans-***4**. Enantioresolution of *trans*-**4** was achieved by preparative HPLC using a Chiralpack OD column as the stationary phase and a mixture of *n*-hexane:*i*-propanol in a ratio 99.95:0.05 as the eluent. (3*R*,3′*R*)-(*P*,*P*)-*trans*-**4**: UV−vis (*n*-hexane) λ_{max} (ϵ) 222 (85 700), 236 (64 400), 312 (14 600), 338 (13 200); CD (*n*-hexane) λ_{max} ($\Delta\epsilon$) 218.0 (+154.9), 224.2 (+37.8), 228.6 (+82.2), 239.4 (−69.0), 252.6 (+82.1), 308.2 (−16.2). Maximum of fluorescence by irradiation at λ = 344 nm: λ = 374 nm.

(3*S,3′*S**)-(*M**,*M**)-*trans*-1,1′,2,2′,3,3′,4,4′-Octahydro-3,3′-di-*i*-propyl-7,7′-dimethyl-4,4′-biphenanthrylidene (4).** A solution of stable **4** in benzene-d_6 or toluene-d_8 was irradiated overnight at 10 °C with a Hg-lamp using wavelengths $\lambda \geq$ 280 nm. After irradiation, stable *trans*-**4** was found to be converted to the unstable *trans*-**4**; ^{1}H (300 MHz, $CDCl_3$) δ 0.04−0.06 (d, J = 6.6 Hz, 6H), 0.62−0.64 (d, J = 6.6 Hz, 6H), 1.00−1.12 (m, 2H), 1.22−1.40 (m, 2H), 1.84−1.96 (m, 2H), 2.48 (s, 6H), 2.54−2.75 (m, 6H), 7.21−7.28 (m, 4H), 7.63 (s, 2H), 7.64−7.67 (d, J = 8.1 Hz, 2H), 8.35−8.38 (d, J = 8.8 Hz, 2H); ^{1}H (300 MHz, C_6D_6) δ 0.23−0.25 (d, J = 7.0 Hz, 6H), 0.77−0.80 (d, J = 7.0 Hz, 6H), 1.35−1.49 (m, 4H), 1.87−1.94 (m, 2H), 2.27 (s, 6H), 2.47−2.55 (m, 2H), 2.79−2.88 (m, 2H), 3.03−3.05 (m, 2H), 7.13−7.15 (d, J = 8.8 Hz, 2H), 7.20−7.22 (d, J = 8.1 Hz, 2H), 7.54 (s, 2H), 7.61−7.63 (d, J = 8.1 Hz, 2H), 8.68−8.71 (d, J = 8.8 Hz, 2H); ^{1}H (400 MHz, C_7D_8) δ 0.19−0.21 (d, J = 7.0 Hz, 6H), 0.74−0.76 (d, J = 7.0 Hz, 6H), 1.32−1.42 (m, 4H), 1.87−1.93 (m, 2H), 2.28 (s, 6H), 2.47−2.52 (dt, J = 14.6, 3.0 Hz, 2H), 2.77−2.85 (dt, J = 13.9, 3.0 Hz, 2H), 2.97−2.99 (d, J = 8.8 Hz, 2H), 7.11−7.14 (dd, J = 8.8, 1.5 Hz, 2H), 7.15−7.17 (d, J = 8.1 Hz, 2H), 7.48 (s, 2H), 7.55−7.57 (d, J = 8.1 Hz, 2H), 8.60−8.62 (d, J = 8.8 Hz, 2H); ^{13}C (75 MHz, $CDCl_3$) δ 17.3 (q), 21.2 (q), 22.1 (q), 23.5 (t), 29.4 (d), 31.2 (t), 45.4 (d), 125.9 (d), 126.2 (d), 126.9 (d), 127.7 (d), 128.2 (d), 129.1 (s), 133.3 (s), 133.6 (s), 136.5 (s), 136.6 (s), 140.7 (s); ^{13}C (75 MHz, C_6D_6) δ 17.6 (q), 21.2 (q), 22.4 (q), 23.9 (t), 29.8 (d), 31.7 (t), 46.1 (d), 126.3 (d), 126.6 (d), 128.7 (d), 129.9 (s), 133.8 (s), 134.1 (s), 137.0 (s), 137.1 (s), 141.0 (s); two (d) were not observed due to overlap of the solvent; (3*R*,3*R*′)-(*M*,*M*)-*trans*-**4**: UV−vis (*n*-hexane) λ_{max} (ϵ) 223 (82 800), 249 (25 800), 367 (11 000); CD (*n*-hexane) λ_{max} ($\Delta\epsilon$) 220.2 (−134.2), 226.2 (+109.7), 244.6 (−38.5), 254.0 (+10.8), 273.8 (−22.0), 360.6 (+26.4). Maximum of fluorescence by irradiation at λ = 344 nm: λ = 568 nm.

(3*S,3′*S**)-(*P**,*M**)-*trans*-1,1′,2,2′,3,3′,4,4′-Octahydro-3,3′-di-*i*-propyl-7,7′-dimethyl-4,4′-biphenanthrylidene (4).** This isomer of **4** was obtained pure by irradiation of the stable *trans*-**4** in toluene-d_8. When ^{1}H NMR indicated that the conversion was complete, the sample was heated at 70 °C for 4 d, until the sample consisted of approximately 75% of the unstable (3*S**,3′*S**)-(*P**,*M**)-*trans*-**4**. The toluene-d_8 was then removed under reduced pressure, and the light yellow solid was recrystallized from heptane giving the (3*S**,3′*S**)-(*P**,*M**)-*trans*-**4** as white crystals, suitable for X-ray analysis, in a very small amount; ^{1}H (400 MHz, $CDCl_3$) δ 0.32−0.34 (d, J = 6.2 Hz, 3H), 0.36−0.38 (d, J = 6.6 Hz, 3H), 0.38−0.40 (d, J = 6.2 Hz, 3H), 0.50−0.52 (d, J = 6.2 Hz,3H), 0.62−0.74 (m, 1H), 0.88−0.99 (m, 1H), 1.18−1.25 (m, 1H), 1.66−1.74 (q, J = 11.5 Hz, 1H), 1.85−1.95 (m, 1H), 2.20−2.35 (m, 2H), 2.53 (s, 3H), 2.54 (s, 3H), 2.65−2.75 (m, 1H), 2.84−2.88 (dd, J = 13.6, 4.0 Hz, 1H), 2.92−3.05 (m, 2H), 3.38−3.47 (m, 1H), 7.34−7.38 (m, 4H), 7.61 (s, 1H), 7.64−7.67 (m, 3H), 8.07−8.09 (d, J = 8.8 Hz, 1H), 8.34−8.36 (d, J = 8.4 Hz, 1H). The ^{1}H NMR data presented for toluene-d_8 were derived by comparison of a spectrum containing a mixture of (3*S**,3′*S**)-(*P**,*P**)-*trans*-**4** and (3*S**,3′*S**)-(*P**,*M**)-*trans*-**4** with the spectra of (3*S**,3′*S**)-(*P**,*P**)-*trans*-**4** and (3*S**,3′*S**)-(*M**,*M**)-*trans*-**4**. ^{1}H (400 MHz, toluene-d_8) δ 0.29−0.30 (d, J = 5.9 Hz, 3H), 0.32−0.34 (d, J = 6.6 Hz, 3H), 0.50−0.51 (d, J = 5.9 Hz, 3H), 0.67 (br s, 3H), 1.17−1.26 (m, 3H), 1.68−1.75 (q, J = 10.0 Hz, 1H), 1.78−1.92 (m, 1H), 2.28 (s, 3H), 2.32 (s, 3H), 2.34−2.49 (m, 2H), 2.75−2.81 (m, 1H), 2.86−2.91 (dd, J = 14.5, 7.9 Hz, 1H), 2.95−3.00 (m, 1H), 3.12−3.20 (dt, J = 13.4, 6.2 Hz, 1H), 3.54−3.63 (m, 1H), 7.20−7.29 (m, 3H), 7.32−7.34 (m, 1H), 7.41 (s, 1H), 7.49 (s, 1H), 7.55−7.57 (d, J = 8.4 Hz, 1H), 7.58−7.60 (d, J = 8.4 Hz, 1H), 8.27−8.29 (d, J = 8.4 Hz, 1H), 8.53−8.55 (d, J = 8.4 Hz, 1H); ^{13}C (100 MHz, $CDCl_3$) δ 20.3 (q), 21.4 (q), 21.50 (q), 21.55 (q), 21.7 (q), 22.6 (q), 26.0 (t), 27.4 (t), 28.5 (d), 29.5 (t), 30.9 (t), 33.7 (d), 47.9 (d), 53.4 (d), 124.9 (d), 125.4 (d), 125.5 (d), 125.7 (d), 126.1 (d), 126.7 (d), 127.1 (s), 127.3 (d), 127.4 (d), 127.6 (d), 127.8 (d), 131.2 (s), 132.2 (s), 132.4 (s), 132.5 (s), 133.8 (s), 133.9 (s), 135.9 (s), 136.4 (s), 136.5 (s), 137.8 (s), 142.8 (s). UV−vis: (*n*-hexane) λ_{max} (ϵ) 229 (83 500), 302 (12 900), 331 (7800).

Acknowledgment. Financial support from The Netherlands Foundation for Scientific Research (NWO-CW) is gratefully acknowledged.

Supporting Information Available: Experimental procedures for the synthesis and the physical properties of compounds **7**−**17**; detailed data for the X-ray structures of (3*S*,3′*S*)-(*M*,*M*)-*trans*-**2**, (3*S*,3′*S*)-(*M*,*M*)-*cis*-**2**, (3*R**,3′*R**)-(*P**,*P**)-*trans*-**3**, (3*R**,3′*R**)-(*P**,*P**)-*cis*-**3**, (3*S**,3′*S**)-(*P**,*P**)-*trans*-**4**, (3*S**,3′*S**)-(*M**,*M**)-*trans*-**4**, and (3*S**,3′*S**)-(*P**,*M**)-*trans*-**4**; crystallographic information files (CIF); Eyring plots of thermal helix inversions of both the *cis*- and the *trans*-isomers of molecules **2** and **3**; details for the rotary cycle of the ethyl substituted molecular motor **2**; fluorescence spectra; mathematical fitting of the thermal helix inversion observed for the *trans*-isomers of **4**. This material is available free of charge via the Internet at http://pubs.acs.org.

JA052201E